Title
Structural and mechanistic insights into the regulation of cellular quiescence by Rb and p130

Permalink
https://escholarship.org/uc/item/0qx721kp

Author
Hirschi, Alexander

Publication Date
2013

Peer reviewed|Thesis/dissertation

UNIVERSITY OF CALIFORNIA
SANTA CRUZ

**STRUCTURAL AND MECHANISTIC INSIGHTS INTO THE REGULATION
OF CELLULAR QUIESCENCE BY RB AND P130**

A dissertation submitted in partial satisfaction of the requirements for the degree of

DOCTOR OF PHILOSOPHY

in

MOLECULAR, CELL, AND DEVELOPMENTAL BIOLOGY

by

Alexander Hirschi

June 2013

The dissertation of Alexander Hirschi is approved:

_____

Professor Seth M. Rubin, chair

_____

Professor Doug Kellogg

_____

Professor Susan Strome

_____

Tyrus Miller
Vice Provost and Dean of Graduate Studies

Table of Contents

Chapter 1

Regulation of cell growth and division by the pocket protein family

Results

Chapter 2

An overlapping kinase and phosphatase docking site regulates activity of the

retinoblastoma tumor suppressor protein

Results

Materials and Methods

Chapter 3

Structural and functional characterization of the MuvB core

Results

Materials and Methods

Bibliography

List of Figures

List of Tables

Abstract

Alexander Hirschi

Structural and mechanistic insights into the regulation of cellular quiescence by

Rb and p130

The ability of a single cell to grow, replicate its genetic material, and divide into two identical daughter cells is a vital process to ensure the propagation of all life. This process is known as the cell division cycle (cell cycle) and is one of the most highly spatially and temporally regulated cellular processes. Misregulation of the cell cycle, particularly in ways that confer both a proliferative advantage and escape from ultimate growth control mechanisms like cellular senescence or apoptosis, can result in unrestrained cell division and tumor formation. In this study, I utilize structural biology, biochemistry, and biophysical data to demonstrate a novel mechanism regulating Rb phosphorylation state and to map pairwise interactions in a conserved cell-cycle regulatory complex called the MuvB Core. First, competition between CDK and PP1 for Rb access provides an efficient regulatory mechanism to dephosphorylate Rb during mitotic exit and times of genotoxic stress. Second, data is presented mapping domain contacts in the MuvB Core, and structure/function studies with MuvB Core suggest an atypical function in regulation of chromatin structure.

Acknowledgements

<p align="center">**Chapter 1**</p>

<p align="center">**Regulation of cell growth and division by the pocket protein family**</p>

Introduction

The ability of a single cell to grow, replicate its genetic material, and divide into two identical daughter cells is a vital process to ensure the propagation of all life. This process is known as the cell division cycle (cell cycle) and is one of the most highly spatially and temporally regulated cellular processes. Misregulation of the cell cycle, particularly in ways that confer both a proliferative advantage and escape from ultimate growth control mechanisms like cellular senescence or apoptosis, can result in unrestrained cell division and tumor formation.

Historically, the prevalent models of tumorigenesis attributed aberrant cell proliferation to mutant, constitutively active growth factors known as oncogenes (Hanahan & Weinberg, 2011). However, this model was turned on its head with the discovery of a factor that, when lost, promoted cell growth. These genetic factors, now called tumor suppressors, negatively regulate cell growth; their loss can confer significant proliferative advantage to a dividing cell.

RB1 was the first tumor suppressor gene to be cloned (Lee et al., 1987), spurred by Alfred Knudson's now-famous "two-hit hypothesis" (Knudson, 1971). In this hypothesis, Knudson proposed that individuals with familial retinoblastoma (eventually giving RB1 its name) inherited an absent or non-functional copy of an important tumor suppressor gene, predisposing them to cancer, which is ultimately

<p align="center">1</p>

caused by a sporadic "second hit" to the remaining copy of this gene in early development. While retinoblastoma itself is a fairly rare disease and treatable in developed nations, we now know that the product of RB1, the retinoblastoma tumor suppressor protein (Rb), is absent or misregulated in most human cancers, suggesting a central role in tumor suppression (Sherr & McCormick, 2002).

Rb interacts with E2F family transcription factors

Rb is composed of structured N-terminal (RbN) and "pocket" domains separated by a flexible linker, as well as a flexible C-terminus (RbC). Rb negatively regulates cell growth by physically interacting with E2F family transcription factors during the early G1 phase of the cell cycle, preventing them from recruiting the transcription pre-initiation complex (PIC) and entering S phase (Hagemeier, Cook, & Kouzarides, 1993; Hiebert, Chellappan, Horowitz, & Nevins, 1992). While there are at least eight E2F subunits and two DP subunits, each capable of eliciting a different transcriptional response while binding to the same nucleotide sequence upstream of E2F target genes (Chen, Tsai, & Leone, 2009; Trimarchi & Lees, 2002), Rb displays *in vivo* specificity for the 'activator' E2Fs 1, 2, and 3a (Trimarchi & Lees, 2002).

Rb binds E2Fs via two distinct modes; the pocket domain binds the E2F transactivation domain (E2F TD), while RbC interacts with the "marked box" domain (C. Lee, Chang, Lee, & Cho, 2002a; Rubin, Gall, Zheng, & Pavletich, 2005). Both RbC and pocket domains are required for efficient E2F gene repression in cellular

2

assays, while the RbN domain is dispensable for E2F inactivation (Bremner et al., 1995; Hiebert, 1993).

A requirement of Rb-E2F complex formation is that Rb exists in a nuclear, *hypophosphorylated* state, as phosphorylation of Rb weakens its affinity for E2F and causes complex dissociation via an autoinhibitory mechanism (Knudsen & Wang, 1997). Complex dissociation and Rb phosphorylation results in the nuclear export of *hyperphosphorylated* Rb and PIC recruitment by E2F (Jiao, Datta, Lin, Dundr, & Rane, 2006). The timing of Rb phosphorylation is coincident with a critical growth restriction point in the cell cycle, a point near the G1/S boundary after which the cell will continue the division program regardless of the removal of growth factors (Pardee, 1989).

Rb is phosphorylated at up to 16 sites scattered throughout its length. All of these sites are contained within flexible loops and linkers, and many of these sites occur in pairs. This led to a major effort to understand the role (or roles) of these sites in the regulation of Rb activity. While many early studies (often carried out in cells) were frequently contradictory in their findings, more recent structure/function studies have shed a great deal of light on the role of specific phosphorylation sites in Rb inactivation. Briefly, phosphorylation of Ser608 causes a short flexible segment in the pocket domain to fold back and occupy the binding cleft normally occupied by the E2F TD, while phosphorylation of T373 induces an interaction between the pocket domain and RbN that pries open the E2F TD binding cleft, reducing E2F TD affinity

for the pocket domain (Burke, Deshong, Pelton, & Rubin, 2010; Burke, Hura, & Rubin, 2012). Additionally, phosphorylation of RbC at Ser788, Ser795, Thr821 and Thr826 causes dissociation of RbC from the E2F marked box domain (Rubin et al., 2005).

Rb is phosphorylated in a cell cycle-dependent manner by the coordinated action of serine/threonine kinases called cyclin-dependent kinases (CDKs), whose activity is low or absent in a quiescent or terminally differentiated cell due to the absence of their activating cyclin partners. This results in Rb hypophosphorylation, Rb-E2F complex formation, and E2F target gene repression.

Rb regulation by CDKs

Rb is a substrate of all major human CDKs, CDK4/6, CDK2, and CDK1 (Lees, Buchkovich, Marshak, Anderson, & Harlow, 1991; Mittnacht, 1998). Upon the receipt of mitogenic signals, cyclin D expression is induced, and the formation of an active cyclin D-CDK4/6 complex is concomitant with initial Rb phosphorylation events and progression through the G1 phase of the cell cycle. While the exact consequences of these early events is not entirely clear and more functional studies are needed, it has been suggested that these initial phosphorylation events may serve to disengage regulatory proteins (other than E2F) from Rb (Dunaief et al., 1994; Wang, 1996; H. S. Zhang et al., 2000). At the G1/S transition, a spike of cyclin E expression upregulates CDK2 activity, resulting in the disruption of Rb-E2F complexes and passage through the restriction point which separates the mitogen-

dependent phase of the cell cycle (G1) from mitogen-independent phases (S-M). Hyperphosphorylated Rb is maintained via the action of cyclin A-CDK2 (during S/G2) and cyclin B-CDK1 (during G2/M phase) until late anaphase, at which point cyclin B degradation by the ubiquitin-proteasome system and the concomitant action of the ubiquitous serine/threonine protein phosphatase-1 (PP1) results in Rb dephosphorylation, re-association with E2Fs, and cell cycle arrest.

While acute deletion or genetic mutation of RB1 resulting in loss-of-function is present in many cancer types such as retinoblastoma, osteosarcoma, and small cell lung carcinomas (Burkhart & Sage, 2008), there are subsets of cancers that have ostensibly normal copies of RB1. Despite this, these cells display constitutive Rb hyperphosphorylation and happily bypass the restriction point unimpeded. These tumor types often display aberrantly high CDK activity profiles due to increased cyclin levels or loss of CDK inhibition by cellular kinase inhibitors (Hanahan & Weinberg, 2011). This has spurred major efforts over the past two decades to develop CDK inhibitors as potential therapeutic drugs, which in *in vitro* studies showed great promise. Unfortunately clinical trials revealed significant toxicity due to off-target effects, and no CDK inhibitors have ever made it to market as anti-cancer drugs (Malumbres, Pevarello, Barbacid, & Bischoff, 2008). However, the significant focus on the interplay between CDKs and Rb shed a great deal of light upon the mechanisms of Rb inactivation by phosphorylation. Most relevant to this work was the observation that cyclin-CDK complexes physically interact via their cyclin

subunit with a defined motif (the "RxL" motif) in the C-terminus of Rb and that this direct interaction is required for Rb phosphorylation and inactivation *in vivo* (Adams et al., 1999).

Structural studies have shed light on the molecular determinants of RbC RxL interaction with the cyclin A subunit of cyclin A-CDK2, the most important being the burial of Leu875 and Phe877 in a hydrophobic pocket on the surface of cyclin A (Lowe et al., 2002). As all major cell-cycle cyclins (D, E, A, and B) contain the RxL binding patch, it is thought that this interaction is generalizable to all Rb-cyclin-CDK complexes. Importantly, this docking interaction between the Rb RxL motif and cyclin A is distal to both the active site of CDK2 and the majority of phosphoacceptor sites on Rb, a theme that is generalizable to many CDK substrates, particularly those that are multiply phosphorylated (i.e. any protein phosphorylated more than once) (Byrne, Miller, Springer, & O'Shea, 2004). It has been demonstrated that formation of a stable kinase/substrate interaction increases the processive rate of phosphorylation, and that enzyme processivity sharpens cell cycle transitions in mathematical and *in vivo* models (Deshaies & Ferrell, 2001; Nash et al., 2001; Patwardhan & Miller, 2007).

Rb regulation by PP1

Interestingly, a pioneering study revealed that nearly one in four National Cancer Institute tumor cell lines displaying hyperphosphorylated Rb have normal CDK activity profiles. These cells fail to regulate their growth during the later stages

of mitosis when Rb should be enzymatically recycled into the hypophosphorylated state; however, these cells fail to dephosphorylate Rb, which as a result cannot bind E2Fs and suppress their activity (Broceño, Wilkie, & Mittnacht, 2002). The continued presence of hyperphosphorylated Rb in G0/G1 allows these cells to pass the restriction point and continue to proliferate in an unrestrained manner. These studies indicate a clear necessity to understand the mechanisms of Rb dephosphorylation by PP1.

PP1 is a ubiquitous and highly conserved serine/threonine phosphatase

Mammalian PP1 is composed of a catalytic serine and threonine phosphatase subunit (PP1c) with three cellular isoforms (α, β, and δ) differing significantly only at their unstructured N- and C-termini, and usually complexed with any one of hundreds of regulatory subunits that either confer sequence specificity/substrate affinity, restrict activity, or alter PP1c subcellular localization (Ceulemans & Bollen, 2004; Cohen, 2002). PP1c is one of the most conserved enzymes in nature and is present in all cells of all eukaryotes (Cohen, 2002). Even bacteriophage lambda encodes a phosphatase (λ-phosphatase) that is 35% identical (up to 49% similar) to the first 150 residues of PP1, highlighting the ubiquitous nature of this enzyme (Cohen, Collins, Coulson, Berndt, & da Cruz e Silva, 1988).

Regulation of PP1c activity by cellular regulators

As the catalytic subunit of PP1 is a highly promiscuous enzyme (save for its preference for phosphorylated serine/threonine residues), it is thought that the

extreme diversity of regulatory subunits directs PP1c to the correct substrates with the correct timing (Cohen, 2002). For instance, the MYPT1 regulatory subunit confers specificity to PP1c's active site for the light chain of myosin, forming the myosin phosphatase holoenzyme complex (MP) (Terrak, Kerff, Langsetmo, Tao, & Dominguez, 2004). PP1c interacts with its regulatory subunits that contain a conserved "RVxF" motif via a hydrophobic cleft distal to the active site of PP1c. However, various studies quarrel about the formal definition of this motif (Hendrickx et al., 2009; Meiselbach, Sticht, & Enz, 2006; Wakula, Beullens, Ceulemans, Stalmans, & Bollen, 2003). As of 2009, bioinformatic approaches assigned the RVxF motif a degeneracy of $[K_{55}R_{34}][K_{28}R_{26}][V_{94}I_6]\{FIMYDP\}[F_{83}W_{17}]$, where the numbers in subscript indicate the percentage of residue occurrence and braced residues are totally excluded (Hendrickx et al., 2009). However, both this definition and the less-stringent and biochemically-determined Meiselbach et. al (2006) definition ([HKR][ACHKMNQRSTV][V][CHKNQRST][FW]) erroneously exclude many known interactors, some of which have been structurally characterized as having an RVxF motif (e.g. inhibitor-2) (Hurley et al., 2007; Meiselbach et al., 2006). Clearly, in order to understand the complete repertoire and functional diversity of PP1c regulatory subunits, it will be of prime importance to rigorously determine the true degeneracy of the RVxF motif.

Regulation of PP1 activity towards Rb

Given the tight regulation of phosphatase activity within the cell and the continual discovery of new PP1c regulatory subunits, it is perhaps logical to assume the existence of a PP1c regulatory subunit that confers specificity to hyperphosphorylated Rb. It has been reported that MP and a high-molecular weight phosphatase isolated from nuclear fractions dephosphorylate Rb (Kiss et al., 2008; Nelson, Krucher, & Ludlow, 1997). However, the sequence context surrounding the sixteen Rb phospho-sites are drastically different, and given that PP1c regulatory subunits are supposed to increase specificity, it seems unlikely that a regulatory subunit would be involved. In support of this notion, there have been several reports indicating a direct interaction between Rb and all three isoforms of PP1c, and that the free catalytic subunit displays Rb phosphatase activity (Tamrakar & Ludlow, 2000; Vietri, Bianchi, Ludlow, Mittnacht, & Villa-Moruzzi, 2006). In these studies, RbC was *required* for Rb-PP1c complex formation. , supporting the hypothesis that a direct interaction between Rb and PP1c facilitates rapid dephosphorylation of serine/ threonine residues in different chemical environments.

Given the opposing conclusions of these studies, the mechanism of Rb-specific PP1 activity remained unclear. In Chapter 2 of this work, I will describe the molecular details of the RbC-PP1c interaction, as well as my finding that PP1c uses its regulatory subunit-binding cleft to dock with an RVxF motif in RbC. The PP1c binding sequence overlaps with the previously identified RxL cyclin binding site, and the association of Rb with PP1c or cyclin-CDK is mutually exclusive. These results

reveal an efficient regulatory mechanism in which phosphatase and kinase activities affect phosphorylation state not only through catalysis but also through restricting access to their target substrate.

Rb and chromatin

While the ability of Rb to interact with E2Fs in a phosphorylation-dependent manner is a critical determinant of cell cycle progression, a separate line of research has suggested that Rb's tumor suppressive functions may be separable from its function at the G1/S restriction point. The basis for this theory comes from work indicating that a highly conserved "LxCxE" motif binding site in the pocket domain of Rb is dispensable for Rb-E2F interaction (Dick, Sailhamer, & Dyson, 2000), but LxCxE binding site mutants of Rb display an inability to recruit histone deacetylases (HDACs) and decreased transcriptional repression in cell-based assays (Dahiya, Gavin, Luo, & Dean, 2000). In a cellular context, actively transcribed euchromatic regions are characterized by an increase in histone acetylation, and removal of these groups by HDAC activity is implicated in chromatin compaction, decreased promoter accessibility to the transcription machinery, and transcriptional repression. In mouse models, Rb LxCxE mutant mice are viable and fertile, but phenocopy heterochromatic abnormalities present in pocket protein triple knockout (Rb, p107, and p130 -/-) mouse embryos, which fail to survive gestation (Isaac et al., 2006). Long-term studies in these models demonstrate that Rb LxCxE mutant mice are tumor-prone. This suggests that Rb's ability to recruit chromatin modifiers (and

potentially many other LxCxE containing regulators) plays an important role in the formation of heterochromatin, genomic stability, and long-term tumor suppression, as well as the regulation of cellular senescence (Talluri et al., 2010).

Paradoxically, Rb coverage of E2F target gene promoters in quiescent or terminally differentiated cells is low; rather the structural and functional Rb homolog p130 (in a complex with the repressor E2F4) dominates at both the total protein level (Henley & Dick, 2012) and at promoter coverage by chromatin immunoprecipitation (ChIP) assay, with p130 residing at over 800 human genes (Litovchick et al., 2007). In spite of this fact, both p130 and its close homolog p107 (which is almost undetectable in quiescent cells) have yet to be implicated in tumorigenesis (Cobrinik, 2005).

This confounding observation is at least partially rectified by two independent lines of evidence. First, the observation that E2F4 loss in Rb -/- mice suppresses tumorigenesis suggests that p107 and p130 *can* function as tumor suppressors if they are freed to interact with the activator E2Fs, presumably by mass action due to E2F4 (the most abundant cellular E2F) loss (E. Y. Lee et al., 2002b). Second, Rb and one of its activator E2F partners, E2F1, play a unique role in the regulation of cellular apoptosis (Rogoff & Kowalik, 2004). Finally, it is formally possible that Rb, p107, and p130 recruit different factors under different cell cycle withdrawal conditions (Rayman et al., 2002). However, there are abundant technical challenges that will need to be addressed before any unified theory regarding pocket protein function and

mechanism of action can be reached. First, ChIP assays are hampered by the fact that endogenous pocket proteins fail to be efficiently recognized by a panel of antibodies following formaldehyde fixation (Stengel et al., 2009). Second, as pocket protein association with both E2F target gene promoters and E2Fs themselves appear to shift in response to cell cycle stage or stimulus, a comprehensive, time-resolved occupancy study will be required to definitively address which pocket proteins (and regulators) are at which promoters, and when. Last, given the fact that Rb, p107, and p130 display both overlapping and unique functions, studies in knockout animals likely have unforeseen complications that confound interpretation of the data. Despite these many caveats, the abundance and presence of p130 at so many E2F target gene promoters suggests an important role in cell cycle regulation, if not necessarily tumor suppression.

Discovery of an ancient cell cycle regulatory complex

How does p130 regulate E2F target genes? Similar to Rb, p130 binds E2Fs, represses transcription, and possesses a highly conserved LxCxE binding cleft. Yet in 2004 extensive biochemical fractionation of *Drosophila* embryo extracts for RBF1 and 2 activity (the *Drosophila* pocket proteins) failed to identify stoichiometric association of chromatin modifiers (Korenjak et al., 2004). Instead, this analysis revealed the presence of a large complex, and fully seven of its eight members were from the synthetic multi-vulvae B (SynMuvB) class of genes identified in pioneering genetic screens in *C. elegans*, suggesting extensive evolutionary conservation of

specific Rb-repressor complexes (Ceol & Horvitz, 2001; Ferguson & Horvitz, 1989; Horvitz & Sulston, 1980). These proteins, together known as 'dREAM' (*Drosophila* RBF, E2F, and Myb) have clear homologs in mammals, and MuDPIT analysis of p130 IPs in human cells identified five stably associated MuvB proteins, confirming the evolutionary conservation of a dREAM complex core (Litovchick et al., 2007).

Composition of DREAM

These five human MuvB proteins (lin9, lin37, RbAp48, lin52, and lin54, hereafter termed the 'MuvB core') stably associate throughout the cell cycle, as IPs from cells synchronized different cell cycle phases indicate MuvB core formation. Yet, p130/E2F4 association is lost after the G1/S transition, presumably in a p130-phosphorylation dependent manner (perhaps similar to the mechanism of Rb-E2F dissociation). Instead, the MuvB core associates with the transcription factors B-Myb (forming the Myb-MuvB complex or MMB) and FOXM1, which is required for the proper expression of mitotic genes and passage through G2/M (Knight, Notaridou, & Watson, 2009; Sadasivam, Duan, & DeCaprio, 2012). Interestingly, *Drosophila* Myb was detected by Korenjak et al. (2004) in their biochemical fractionations, but no *C. elegans* Myb homolog has been discovered. This suggests that either a cryptic *C. elegans* Myb homolog has yet to be discovered or that MuvB underwent a gain-of-function in G2/M gene regulation during evolution. Until data exist to resolve this question, any hypothesis remains speculative. RNAi-mediated knockdown of human 'DREAM' (DP, Rb, E2F, and MuvB) components in human cells upregulates cell

cycle genes in arrested cells. MuDPIT analysis of DREAM complex IPs from human cells failed to identify the presence of chromatin modifiers, leaving the mechanism of DREAM action a mystery (Litovchick et al., 2007).

Functions of some MuvB members are known. RbAp48 (p48) is a well-characterized WD40 propeller domain with histone reader and nucleosome chaperone functions (depending on the context). It is found in other regulatory complexes such as Polycomb Repressive Complex 2 (PRC2) and Nucleosome Remodeling and Deacetylation complex (NuRD). lin54 has been recently characterized as a DNA-binding protein involved in localizing DREAM and MMB to cell-cycle homology (CHR) elements in the genome (Schmit, Cremer, & Gaubatz, 2009; Tabuchi et al., 2011). lin9, lin37, and lin52 remain uncharacterized, although lin9 contains a putative tudor domain, and phosphorylation of lin52 at Ser28 by the DRK1A kinase appears to be required for DREAM complex formation *in vivo* (Litovchick, Florens, Swanson, Washburn, & DeCaprio, 2011).

In Chapter 3 of this work, I will describe the initial efforts of our lab to structurally characterize the heteropentameric MuvB core in an attempt to elucidate the mechanism of gene repression by DREAM. I present the results of pairwise-interaction studies that shed light on the gross structural architecture of the MuvB core and that predict the presence of stable subdomains that may be more amenable to structural studies than the entirety of MuvB or DREAM/MMB. Additionally I present the high-resolution structure of the putative tudor domain in lin9, and attempts to

characterize its function via NMR titrations, biochemical pulldowns, and peptide array-based assays.

Chapter 2

An overlapping kinase and phosphatase docking site regulates activity of the retinoblastoma tumor suppressor protein

Introduction

Historically, inquiries into mechanisms regulating Rb phosphorylation have focused on the modulation of CDK activity (Dyson, 1998; Morgan, 1995; Weinberg, 1995). Rb phosphorylation is generally coincident with high levels of CDK activity, but there are circumstances such as mitotic exit and cell cycle arrest following acute DNA damage, when Rb must be actively dephosphorylated and maintained in a hypophosphorylated state despite the presence of residual kinase activity. In fact, several cancer cell lines were shown to be defective in the activation of Rb by dephosphorylation (Broceño et al., 2002). A direct interaction has been observed between PP1c and RbC, and this interaction was required for Rb-directed phosphatase activity in a number of *in vitro* and cellular assays (Tamrakar & Ludlow, 2000; Vietri et al., 2006). Furthermore, stable Rb-PP1 complexes have been observed that are coincident with the dephosphorylation of Rb in mitosis (Durfee et al., 1993), and work by Wu et al. (2009) suggests the release of free, active catalytic subunit from PP1c-Inhibitor-1 complexes is responsible for the dephosphorylation of many mitotic phosphoproteins upon exit from mitosis (Wu et al., 2009). Despite reports to the

contrary (Kiss et al., 2008; Nelson et al., 1997), a bulk of evidence points to a direct, functional interaction between RbC and PP1c, motivating my studies to elucidate the molecular details of this interaction.

Results

Rb$^{870-882}$ is necessary and sufficient for Rb-PP1c association

To determine the precise sequence requirements for RbC-PP1c binding, we used isothermal titration calorimetry (ITC) to quantify binding affinity between PP1c and Rb. We titrated recombinant, purified Rb$^{55-928}$ (containing all conserved Rb domains and phosphoacceptor sites, Figure 1a) into recombinant PP1c (α-isoform, used for all following experiments) and calculated the dissociation constant from the resulting binding isotherm (Figure 1b). This Rb construct binds PP1c with $K_d = 3.9 \pm 0.2$ µM, giving us our baseline Rb-PP1c affinity. This value in the low micromolar range is fairly typical of enzyme-substrate interactions, and is similar to that observed between RbC and cyclin A (Lowe et al., 2002). Next we titrated a series of RbC truncation mutants into PP1c and calculated their affinity from the resulting isotherms (Figure 1 c-g). RbC$^{771-928}$ and RbC$^{866-928}$ bound PP1c with similar affinities to that of Rb$^{55-928}$, which is consistent with previous reports that RbC is both necessary and sufficient for Rb-PP1 association, and that Rb phosphorylation is not required (Egloff, Cohen, Reinemer, & Barford, 1995; Tamrakar & Ludlow, 2000; Vietri et al., 2006). Titration of Rb$^{889-928}$ into PP1c resulted in total loss of binding signal, indicating that at least part of the molecular determinant of Rb-PP1C interaction lies between Rb

16

residues 866 and 889. With a synthetic peptide corresponding to Rb residues 870-882, we found that we were able to recapitulate Rb$^{55-928}$-PP1c affinity, confirming that this short Rb$^{870-882}$ sequence contains all significant interacting residues. This conserved sequence contains the defined cyclin A RxL docking motif, and a Lys-Leu-Arg-Phe (KLRF) sequence that closely resembles the consensus RVxF motif found in PP1c regulatory subunits (Figure 2). Notably, this KLRF sequence is not predicted by the degenerate RVxF motif definition (Meiselbach et al., 2006; Wakula et al., 2003), as mutation of valine in position -2 (relative to phenylalanine) to leucine in the mammalian glutamate receptor (mGluR) RVxF motif abolished mGluR-PP1c interaction (Meiselbach et al., 2006). Similarly, the presence of leucine in the -2 position has never been observed in global approaches to defining the PP1c-RVxF interactome (Hendrickx et al., 2009). Because of the discrepancy between the definition of the RVxF motif and the putative RVxF motif identified in Rb$^{870-882}$, we decided to structurally characterize the interaction between Rb$^{870-882}$ and PP1c.

Crystal structure of an Rb$^{870-882}$-PP1c complex

A PP1c and RbC$^{870-882}$ complex readily crystallized in a variety of conditions in the initial screens, yet repeated trips to the synchrotron following crystal reproduction and optimization failed to yield diffraction quality data. Eventually, we decided to remove the last 30 amino acids from the C-terminus of PP1c, as these amino acids are predicted to be unstructured, are rarely seen in PP1c structures, and are poorly conserved between PP1c isoforms. This construct (PP1c$^{1-300}$) and Rb$^{870-882}$

also crystallized readily and in similar conditions, and the structure was solved to 3.2Å. Statistics for the final model build quality are presented in Table 1, and the overall fold is presented in Figure 3a. The structure of PP1c in this complex is equivalent to that of the PP1c-microcystin and PP1c-tungstate complexes, demonstrating that RbC$^{870\text{-}882}$ fails to induce significant structural changes in the catalytic subunit (Egloff et al., 1995; Goldberg et al., 1995).

The RbC peptide binds to PP1c in an extended conformation at the hydrophobic interface of two β-sheets ("β-sandwich") distal to the PP1c active site (Figure 3a). Binding is mediated by both main chain hydrogen bonding between RbC$^{870\text{-}882}$ and PP1c and hydrophobic side chain interactions (Figure 3b,c). Arg876-Asp878 of Rb$^{870\text{-}882}$ form a short β-strand that adds to sheet 1 of the PP1c β-sandwich, forming an H-bonding pattern similar to that seen in parallel strand-strand interactions.

The other significant interactions between Rb and PP1c are made by the highly conserved Rb side chains of Leu875 and Phe877. These hydrophobic side chains are buried in a pocket formed at the β-sandwich interface, which is conserved between all three PP1c isoforms (Figure 4). These structural data are consistent with the observations that Rb can interact with all three cellular PP1c isoforms (Vietri et al., 2006), and that neither Rb phosphorylation state nor PP1c activity affects Rb-PP1c interaction *in vivo* (Tamrakar, Mittnacht, & Ludlow, 1999).

The location of the Rb-PP1c interaction and the molecular interactions stabilizing the complex are virtually identical to those observed between PP1c and the RVxF motif found in the PP1 targeting subunit MYPT1 (Terrak et al., 2004). In this structure, Lys37-Asp39 of MYPT1 adds to PP1c sheet 1 (δ-isoform) as a parallel β-strand, and Val36 and Phe38 are buried in the same hydrophobic pocket as Leu875 and Phe877 of Rb (Figure 5a).

It is important to note that Leu875 and Phe877 of Rb also bind to a hydrophobic pocket in the surface of cyclin A (Figure 5b) (Lowe et al., 2002), and that Leu875 is required for efficient phosphorylation of Rb (Adams et al., 1999; Lowe et al., 2002; Schulman, Lindstrom, & Harlow, 1998). Both L875 and Phe877 appear critical to stabilize the observed docking interaction between RbC and CDK or PP1c, suggesting that kinase or phosphatase binding to the overlapping RxL/RVxF motifs would be mutually exclusive. However, it is a formal possibility that L875 might bind kinase, and Phe877 might simultaneously bind phosphatase, or vice versa. Mutation of these residues (L875R and F877A) in an Rb$^{866-928}$ construct followed by ITC binding studies with PP1c and cyclin A-CDK2 revealed a total loss of binding of both mutants to both enzymes (Figure 6). These data verify that Leu875 and Phe877 are part of an enzyme docking site in Rb required for interaction with both kinase and phosphatase, and strongly predict that binding of one enzyme to Rb will exclude the other.

The Rb paralogs p107 and p130 also contain RxL sequences that are critical for binding to cyclin A-CDK2 (Lowe et al., 2002; Schulman et al., 1998). However, unlike Rb, the phenylalanine in both the p107 and p130 docking motifs directly follows the leucine (Arg-Arg-Leu-Phe). We found that the cyclin binding motifs in both p107$^{655-667}$ and p130$^{677-689}$ do not also bind PP1c (Figure 7). This result is consistent with the crystal structure, which revealed that leucine forms critical contacts with PP1c in the −2 position relative to phenylalanine.

PP1c docking is required for efficient RbC dephosphorylation

To examine the effects of the Rb-PP1c interaction on Rb-directed PP1c phosphatase activity, we developed kinetic assays to measure Rb dephosphorylation rates. We quantitatively phosphorylated RbC constructs with (Rb$^{771-928}$) and without (Rb$^{771-874}$) the overlapping kinase/phosphatse docking site, each containing seven CDK consensus sites, with 32P (Figure 8a). After mixing phosphorylated RbC (phosRbC) constructs with PP1c, we measured the loss of signal intensity over time in order to extract kinetic parameters. Signal intensity remained at longer time points in the phosRbC771-874 experiment compared to phosRbC771-928, indicating a clear loss in dephosphorylation efficiency (Figure 8b). Quantification of the signal indicates that the first-order rate constant for dephosphorylation of phosRbC771-874 (k_{dephos} = 0.027 ± 0.002 min^{-1}) is approximately eight times smaller than for phosRbC771-928 (k_{dephos} = 0.200 ± 0.010 min^{-1}) (Figure 8c). It is a formal possibility that deletion of the phosphatase docking site deleteriously affects substrate properties,

therefore artificially affecting the kinetic rate of RbC dephosphorylation. To test this possibility, we repeated phosphatase assays with phosRbC[771-928] in the presence of saturating amounts of an RbC[866-890] peptide containing the docking site. This peptide strongly inhibited phosRbC dephosphorylation, confirming that the docking site directs more efficient substrate processing (Figure 8d). Phosphatase assays with mutant phosRbC fragments that contain only one pair of phosphorylated sites show that dephosphorylation occurs at all of the sites with similar kinetics that are sensitive to the presence of the phosphatase docking site (Figure 9).

We performed the phosphatase assays at different substrate concentrations to determine apparent steady-state kinetic parameters for dephosphorylation of the phosRbC sites (Figure 10). The apparent k_{cat} for dephosphorylation of phosRbC[771-874] (k_{cat} = 140 ± 20 min^{-1}) and phosRbC[771-928] (k_{cat} = 160 ± 20 min^{-1}) are similar. However, the apparent Km value for phosRbC[771-874] (Km = 30 ± 10 μM) is greater than that of phosRbC[771-928] (Km = 6 ± 3 μM). Again, these results are consistent with the RbC docking site enhancing substrate dephosphorylation by enabling PP1c to capture Rb in order to form a stable enzyme-substrate complex.

We next examined how mutations in the overlapping PP1c and cyclin-CDK docking sites affect enzyme activity towards Rb. In phosphatase assays similar to those described above, dephosphorylation of an RbC[771-928] construct containing the F877A mutant (k_{dephos} = 0.071 ± 0.004 min^{-1}) is slower than wild type (k_{dephos} = 0.29 ± 0.03 min^{-1}) (Figure 11a). Switching the position of R876 and F877 (R876F/F877R

"FR mutant") creates a docking site that more closely resembles the p107 and p130 docking sites and also decreases the first order rate constant ($k_{dephos} = 0.067 \pm 0.006$ min^{-1}) (Figure 11a).

In order to test these mutants in kinase assays, we prepared complexes of RbC and the E2F1/DP1 heterodimer to mimic the physiological substrate of CDK. In ITC binding assays the presence of E2F1/DP1 does not appreciably alter the affinity of either PP1c or cyclin A-CDK2 for RbC (Figure 12), indicating that E2F1/DP1-RbC complex formation does not conceal the enzyme docking site. The first order rate constant for phosphorylation of RbC$^{771-928}$ ($k_{phos} = 0.023 \pm 0.001$ min^{-1}) is greater than that for the F877A mutant ($k_{phos} = 0.011 \pm 0.001$ min^{-1}) (Figure 11b). This effect is consistent with the observation that this docking site is required for efficient Rb phosphorylation by cyclin A-CDK2 (Adams et al., 1999). The FR mutant ($k_{phos} = 0.024 \pm 0.001$ min^{-1}) has a first order rate constant nearly identical to that of wild type RbC (Figure 11b), consistent with the observation that cyclin A-CDK2 is capable of docking with both Rb and p107/130-like docking sites (Lowe et al., 2002). Taken together, these kinetic assays demonstrate that both PP1c and cyclin-CDK utilize an overlapping docking site in Rb, but not p107 or p130, and indicate that the FR mutant is a defective PP1c substrate but is a viable CDK substrate.

PP1c inhibits cyclin A-CDK2 activity towards Rb

Our previous work demonstrated that PP1c and cyclin-CDK complexes cannot simultaneously occupy the shared docking site in RbC, and that stable

enzyme-substrate interaction is required for both phosphorylation and dephosphorylation of RbC. For these reasons we hypothesized that each enzyme could act as an inhibitor of the other by preventing stable enzyme-substrate complex formation. We first tested whether inactive PP1c could inhibit the phosphorylation of RbC by cyclin A-CDK2 in the kinase assay (Figure 13). In the absence of PP1c, the first-order rate constant for $Rb^{771-928}$ phosphorylation ($k_{phos} = 0.0185 \pm 0.0001$ min^{-1}) was 11 times greater than that for $Rb^{771-874}$ phosphorylation ($k_{phos} = 0.0017 \pm 0.0001$ min^{-1}). We then carried out kinase reactions in the presence of saturating quantities of PP1c that was irreversibly inhibited at its catalytic site with microcystin (Figure 13). The presence of PP1c–microcystin reduces the rate constant for $Rb^{771-928}$ phosphorylation ($k_{phos} = 0.0051 \pm 0.0001$ min^{-1}) such that it is more similar to the rate constant for $Rb^{771-874}$ phosphorylation. By contrast, PP1c–microcystin has little effect on $Rb^{771-874}$ phosphorylation ($k_{phos} = 0.0013 \pm 0.0001$ min^{-1}). Thus, our data indicate that PP1c directly inhibits RbC phosphorylation by cyclin A-CDK2 and that inhibition is independent of phosphatase activity and dependent on the presence of the KLRF docking site. We have also found, using the phosphatase assay, that cyclin A-CDK2 inhibits RbC-directed PP1c phosphatase activity independent of kinase activity (Figure 14).

Inhibition of CDK access to Rb blocks cell-cycle progression

Having established that CDK and PP1c compete for Rb access, we investigated the functional importance of this competition in the context of cell-cycle

regulation. The human osteosarcoma cell line Saos-2 is deficient for Rb, and Rb re-expression leads to a strong G1 arrest (Huang et al., 1988). Coexpression of cyclin A-CDK2 abrogates this arrest through phosphorylation and inactivation of Rb (Hinds et al., 1992; Zhu et al., 1993). We used this model system to observe the effect of PP1 on CDK regulation of Rb (Figure 15a). We found that the Rb-induced arrest was overcome by cyclin A-CDK2 expression, and it could be largely recovered by expressing PP1c. Notably, coexpression of a catalytically inactive mutant of PP1c (PP1c H248K) also resulted in a restoration of G1 arrest. Omission of Rb from these assays abrogated the PP1c-dependent cell-cycle block, confirming that Rb is the relevant target of enzyme competition. In Figure 15b, the expression levels of PP1c were titrated and reveal that catalytically inactive enzyme is as potent as wild type in blocking cell-cycle advancement under conditions in which Rb expression has been reduced. Based on these cell-cycle control data, we conclude that the competition for substrate access between cyclin A-CDK2 and PP1c on Rb offers an efficient means to control cell proliferation beyond the catalytic regulation of phosphorylation.

We next confirmed that PP1c inhibits phosphorylation of Rb in cells, as in our kinetic analyses, in a manner that is independent of catalytic activity. We used C33A cells to test whether exogenously introduced PP1c could compete with CDKs and block Rb phosphorylation regardless of cell-cycle position effects on enzyme activity (Figure 15c). Ectopically expressed Rb becomes phosphorylated in C33A cells. Expression of a dominant negative CDK2 controls for inhibition of Rb

24

phosphorylation in our analysis, and coexpression of Rb with cyclin A-CDK2 shows the maximum extent of Rb hyperphosphorylation. As predicted, expression of PP1c or catalytically dead PP1c H248K inhibited Rb phosphorylation levels in a dose-dependent manner.

Our kinetic data indicate that the Rb^{FR} mutant is a poor PP1c substrate but a good CDK substrate. We used this mutation to study the importance of the docking site for dephosphorylation and Rb activation in cell-based assays. First, we transfected wild-type Rb and Rb^{FR} into C33A cells with and without also trans-fecting PP1c (Figure 15d). Coexpression of PP1c reduces the observed phosphorylation of wild-type Rb (migrates as a faster, single band), whereas the mutant Rb^{FR} is unaffected by phosphatase expression. This observation suggests that the docking interaction observed in our crystal structure is required in cells for efficient Rb dephosphorylation by PP1c.

We also tested the Rb^{FR} mutant in the Saos-2 cell-cycle arrest assay. Expression of Rb^{FR} in Saos-2 cells gives a less robust arrest in G1 compared to wild type, consistent with the idea that Rb activation requires docking-dependent PP1c dephosphorylation that is defective in this mutant (Figure 15e). Cyclin A-CDK2 expression still inactivates Rb^{FR} as expected because the kinase-docking site remains intact. We also find that, under conditions in which Rb and kinase are expressed, coexpression of PP1c is sufficient to restore the activity of wild-type Rb but is unable

25

to reactivate phosphorylated Rb[FR] (Figure 15f). Taken together, these data highlight a critical role for the KLRF docking site in the regulation of Rb activity.

Stable Rb–PP1 complexes are coincident with Rb activation

The competition for access to Rb between PP1c and cyclin-CDK suggests that Rb and PP1c are in a complex at times when Rb is activated by dephosphorylation. To investigate the relevance of this mechanism of cell-cycle regulation under endogenous conditions, we examined the abundance of Rb–PP1c complexes in CV-1 cells during mitotic exit and in transfected Saos-2 cells that arrest in a PP1-dependent manner in early G1 (Figure 16). We used CV-1 cells because synchronization experiments have shown that PP1 and Rb associate selectively in late mitosis, coincident with Rb dephosphorylation and activation in these cells (Durfee et al., 1993). We first compared the relative level of the endogenous proteins in CV-1 cells with the level of transfected proteins in Saos-2 cells by applying recombinant standards (Figure 16a). We found that the molar quantities of Rb in extracts from CV-1 and Saos-2 transfected cells were equivalent. Considering that the majority of Saos-2 cells are transfected in our experiments, the Rb expression level in the Saos-2 cells is no more than 2 times higher. The level of PP1c in mitotic CV-1 cells was a little less than half as much as that of Rb, whereas the total level of endogenous and exogenously introduced PP1c in arrested Saos-2 cells was approximately equivalent to that of Rb. These observations indicate that our transfection-based assay system closely mimics the levels of endogenous proteins under conditions where Rb is

activated. We next immunoprecipitated Rb complexes from CV-1 and transfected Saos-2 cells and immunoblotted for bound PP1c (Figure 16b). The amount of PP1 coprecipitated from arrested Saos-2 cells is ~30% of the total amount of immunoprecipitated Rb, indicating that one- third of Rb molecules are bound to PP1c when cells are arrested in a PP1-dependent manner. The amount of PP1c coprecipitated with Rb in CV-1 cells is ~2%; however, given that the population of CV-1 cells is actively progressing through mitosis and the limitations of synchronization by shakeoff, this measurement likely underestimates the quantity of Rb–PP1c complex that exists in a cell at the instant of Rb activation. Taken together, these experiments suggest that PP1 can form stable, abundant complexes with Rb at endogenous expression levels. These complexes attenuate the activity of CDKs by blocking their access to Rb and regulate progression through the cell cycle.

Discussion

Although much attention has been paid to the inactivation of Rb by CDK phosphorylation from G1 through mitosis, less is known regarding how Rb is activated by PP1 dephosphorylation during mitotic exit and following cellular stress. We have identified a short sequence in RbC that binds to PP1c directly and is required for efficient Rb-directed PP1 phosphatase activity. Our structural data show that the molecular interactions stabilizing RbC–PP1c are nearly identical to those observed between PP1c and its regulatory subunits. Whereas PP1c typically uses its hydrophobic binding cleft to recruit an additional subunit responsible for substrate

27

binding, here PP1c uses the cleft to recruit Rb substrate directly (Egloff et al., 1997; Terrak et al., 2004). Although uncommon, a direct interaction between PP1c and the PP1 substrate Cdc25 has also been observed in *Xenopus laevis* embryonic extracts (Margolis et al., 2003). Recent data indicate that PP1c dissociates from inhibitors following CDK inactivation during mitosis (Wu et al., 2009). The timing of this population of free PP1c is concurrent with the requirement to dephosphorylate Rb through a direct interaction, and it would be interesting to explore whether other PP1 substrates are dephosphorylated at mitotic exit without a targeting subunit, and whether some of these substrates also possess overlapping kinase and phosphatase docking sites. However, the discovery of putative overlapping docking sites is hampered by the fact that none of the canonical RVxF motif definitions predicted an RVxF motif in RbC. Clearly our data show that leucine is a tolerated residue in the -2 position. This is likely to be context-dependent and an understanding of these dependencies will be required to accurately identify candidate sequences.

The fact that the direct enzyme-substrate association is mediated through the RVxF-binding cleft may explain why an Rb-targeting regulatory subunit has not been identified and is not necessary for Rb dephosphorylation (Vietri et al., 2006). Although the existence of such a subunit cannot be ruled out, our data indicate that both Rb and a hypothetical Rb-targeting subunit could not both occupy the RVxF-binding cleft and that a different mode of Rb–PP1 holoenzyme assembly would be required. However, considering that multiple phosphates in varying sequence contexts

must be hydrolyzed in Rb, it seems reasonable that the Rb phosphatase would not use a targeting subunit to impart a high degree of specificity. RbC closely mimics regulatory subunits in PP1c binding, and it is also tempting to speculate that Rb itself is a PP1c regulatory subunit, either sequestering nuclear PP1c from other activating subunits or regulating PP1c access to other substrates. Notably, it has been reported that RbC can act as a noncompetitive inhibitor of PP1c activity toward a generic substrate (Tamrakar et al., 1999).

Our data, together with previous results, indicate that PP1c and cyclin A-CDK2 bind an overlapping docking site in RbC that is required in each case for efficient enzymatic activity (Adams et al., 1999; Lowe et al., 2002). To our knowledge, this observation is the first example of a PP1c-binding sequence (RVxF or other) having an additional functional role that competes with PP1 activity. As a result of their exclusive associations with substrate, we have shown that cyclin A-CDK2 and PP1c can each directly inhibit the activity of the other enzyme toward Rb. This result reveals a novel mechanism for the regulation of Rb phosphorylation state in which kinase and phosphatase compete for access to substrate. Given the conservation of the RxL binding cleft in cyclin paralogs, it is assumed that the observed competition would exist between PP1 and all cyclin-CDKs that phosphorylate Rb. In contrast, the other Rb family proteins p107 and p130 do not bind PP1c; this competitive mechanism is unique to Rb.

Competition between kinase and phosphatase for controlling the phosphorylation state of a common substrate has been established as an important mechanism in cell signaling, and a theoretical framework has been crafted for how such competition can generate critical signaling properties such as sensitivity, switch-like responses and multiple steady-state outputs (Ferrell, 1996; Goldbeter & Koshland, 1981; Salazar & Höfer, 2006; Thomson & Gunawardena, 2009). However, few experimental observations of these properties have been reported. Our finding of a cyclin-CDK competition with PP1c for Rb as a substrate not only provides a rare example of direct kinase-phosphatase competition but also shows that competition can be for substrate docking as well as catalysis. Notably, the presence of common kinase/phosphatase docking sites in mitogen-activated protein kinases has been observed (Tanoue, Adachi, Moriguchi, & Nishida, 2000), suggesting that competition for substrate binding may have a more general role in signal transduction.

In the context of Rb phosphorylation in cell-cycle control, signaling sensitivity and specificity are critical. From mitosis through G1, the capacity of PP1c to inhibit cyclin-CDK could facilitate efficient Rb dephosphorylation in response to small changes in PP1c concentration and could prevent Rb from being promiscuously rephosphorylated by residual CDK activity. The same holds true in response to cellular stress and cell-cycle exit, and in fact, it has been shown that Rb is dephosphorylated in response to DNA damage despite the presence of active CDKs (Dou, An, & Will, 1995). These regulatory concepts, which would serve to activate

Rb, are supported by our cell-cycle arrest assays. Therefore, our findings establish a biochemical mechanism through which Rb phosphorylation and function can be tightly controlled in the cell by directly competing kinase and phosphatase activities. Further study is necessary to determine what mechanisms influence the outcome of the competition and how access of each enzyme to the docking site is controlled. Considering the observation that the association between Rb and PP1c is direct, the nuclear concentrations of PP1c, free of inhibitors and other targeting subunits, are intriguing possibilities.

Materials and Methods

Protein expression and purification

Recombinant PP1c (α isoform) was expressed in E. coli using a tac promoter; 2 mM $MnCl_2$ was added to the media upon induction. Purification was best achieved using a salt-dependent PP1c- inhibitor-2 association (Z. Zhang, Zhao, Zirattu, Bai, & Lee, 1994). Full-length, human inhibitor-2 was expressed with an N-terminal hexahistidine tag in E. coli. Following cell lysis with 6 M urea, inhibitor-2 was bound to nickel sepharose beads and exchanged to a buffer containing 20 mM Tris, 50 mM NaCl, 15 mM imidazole, 0.4 mM MnCl2, 0.2 mM TCEP and 0.1 mM PMSF (pH 8.0). Cells expressing PP1c were lysed in this same buffer, the cleared lysate was passed over the immobilized inhibitor-2 and PP1c was eluted with lysis buffer containing 1 M NaCl. For crystallography, PP1c was further purified with a Superdex75 column (GE Healthcare) equilibrated in 20 mM Tris, 500 mM NaCl, 2

mM DTT, 0.4 mM MnCl2 (pH 8.0). RbC, Rb[55–928], E2F1-DP1 (RbC binding domains) and cyclin A-CDK2 protein constructs were expressed and purified as described previously (Burke et al., 2010; Rubin et al., 2005; Russo, 1997). The Rb constructs in both the calorimetry and kinetic experiments had N-terminal hexahistidine tags left intact. CDK activating kinase from Saccharomyces cervisiae (Cak) was expressed as a GST fusion protein in E. coli and purified with glutathione sepharose affinity chromatography.

Isothermal titration calorimetry

ITC experiments were performed with a VP-ITC instrument (MicroCal). Typically, 0.5–1 mM of each RbC construct or synthetic RbC peptide was titrated into a 25–50 M solution of PP1c. Experiments were carried out at 25°C in a buffer containing 25 mM Tris, 100 mM NaCl and 1 mM DTT (pH 8.0). Each reported binding constant is the average from 2 or 3 experiments, and the reported error is the s.d. of the K_d from these measurements.

Crystallization and structure determination

Purified PP1c was concentrated to 10 mg ml^{-1} after the Superdex75 column and synthetic Rb[870–882] peptide (Biopeptide Co., Inc.) was added in a 3:1 molar ratio. Crystals were grown using the hanging-drop vapor diffusion method at room temperature (22°C) . The crystallization buffer contained 100 mM HEPES, 200 mM MgCl2 and 18% (w/v) PEG 4000 (pH 7.5) and was mixed in a 1:1 ratio with protein solution. Crystals grew with a needle morphology to dimensions of approximately 50

μm × 50 μm × 500 μm. Crystals were harvested by transferring to a solution

containing 100 mM HEPES, 200 mM MgCl2, 20% (w/v) PEG 4000 and 20% (v/v)

glycerol (pH 7.5) and flash freezing in liquid nitrogen. A molecular replacement

solution was obtained using the PP1c–microcystin crystal structure (PDB 1FJM) as a

search model (Goldberg et al., 1995).

Crystal structure refinement

Initial crystals grown with full length PP1c diffracted to moderate resolution

(~4 Å). We attempted to improve resolution by deleting residues 301-330 from PP1c,

as these residues were not observed in previous PP1c structures and are presumed

disordered (Egloff et al., 1995; Goldberg et al., 1995). Crystals of $Rb^{870-882}$-$PP1c^{1-300}$

grew with the same morphology and unit cell parameters as the crystals using full-

length PP1c but diffracted with improved resolution. $Rb^{870-882}$ binds to $PP1c^{1-300}$ with

the same affinity as full length PP1c as determined by ITC (data not shown).

The highest quality diffraction data were collected from crystals of an $Rb^{870-882}$-

$PP1c^{1-300}$ complex. Diffraction data were collected using Beamline 5.0.1 of the

Advanced Light Source (Lawrence Berkeley National Laboratories). Data were

indexed and scaled with Mosflm and SCALE-IT. The structure was determined with

molecular replacement using PP1c alone as an initial model. Two molecules of PP1c

are observable in the asymmetric unit, and an initial difference electron density map

revealed two significant peaks near each of the two PP1c molecules (Figure 17a). One

peak is near the enzyme active site and corresponds to known, bound Mn^{2+} ions. The

other significant feature in the difference map shows clear density corresponding to seven residues of the Rb$^{870-882}$ peptide. Sidechain density in the center of the initial difference map peak could confidently be assigned to Phe877. Accordingly, the rest of the peptide was fit, and the model of the Rb$^{870-882}$-PP1c complex was further refined (Figure 17b).

The Rb peptide was built into the model with COOT, and the entire model further refined with Phenix using standard rigid body, simulated annealing, and temperature factor refinement routines. The similar structures of the two PP1c molecules in the asymmetric unit motivated the use of noncrystallographic symmetry during refinement. Electron density corresponding to RbC was observed near both PP1c molecules, however, it was significantly more interpretable in one of the two complexes, and only one RbC peptide was included in the model. We believe that the intensity difference in RbC electron density results from different occupancies or dynamics; the peptide built into the more interpretable density makes crystal-packing contacts that may stabilize it, whereas the other density in the other asymmetric unit is solvent exposed.

Phosphatase and kinase assays

Purified cyclin A-CDK2 was first activated by phosphorylation in a reaction containing 10% (w/w) GST-Cak, 10 mM MgCl$_2$ and 5 mM ATP. To prepare for the phosphatase assays, 1 mg of RbC was incubated with 0.25 mg of activated cyclin A-CDK2 for 1 h at room temperature in a buffer containing 50 mM HEPES, 100 mM

NaCl, 10 mM MgCl$_2$, 1 mM ATP and 5 μCi of ^{32}P-labeled ATP (pH 7.5). These reaction conditions give nearly quantitative phosphorylation of CDK consensus sites in RbC (Burke et al., 2010). Reactions were quenched by addition of 8 M urea, and phosRbC was isolated with a nickel-nitrilotriacetic acid spin column (Qiagen). Phosphatase reactions were carried out at room temperature in a buffer containing 50 mM HEPES, 100 mM NaCl and 2 mM MnCl$_2$ (pH 7.5). Reactions were initiated by addition of enzyme. Aliquots were removed at the indicated time point and quenched by mixing with SDS-PAGE loading buffer.

Chapter 3

Structural and functional characterization of the MuvB core

Introduction

To date, most functional studies of DREAM have been carried out using RNA-mediated knockdown of individual DREAM components (Esterlechner et al., 2013; Hauser et al., 2012; Litovchick et al., 2007; 2011). Some of these studies suggest an absolute requirement for lin9 for viability, and that lin9 -/- cells that escape senescence (via Rb inactivation by SV40 T-antigen) are chromosomally unstable (Hauser et al., 2012). Interestingly, shRNA of lin52 in human cells reduces protein levels of lin9 and lin37, suggesting some interdependency of these complex members upon each other (Litovchick et al., 2011). Given this interdependence, it is entirely likely that acute depletion of complex members may have different results in cellular assays compared to point mutations, similar to the way pocket protein knockouts and

LxCxE point mutants behave differently (Isaac et al., 2006). In light of the total absence of mechanistic insight into DREAM function and the unique nature of many MuvB core complex members, it will be critical to obtain structural data in order to interrogate DREAM function in a rational and direct manner, motivating the studies undertaken in this chapter.

Results

Expression and purification of recombinant MuvB core

Without a source of pure, homogenous MuvB core complex, downstream structural analysis would be impossible. Therefore, our first goal was to assay whether we could assemble recombinant MuvB core. Sf9 or Hi5 cells were infected with baculovirus stocks coding for all five MuvB components, and then complexes were purified by a combination of nickel and glutathione affinity. As shown in Figure 18, the MuvB core is expressed and can be purified to near homogeneity as judged by SDS-PAGE. As expression of all complex components is induced with a separate virus, we are able to replicate RNA-knockdown studies of whole components (or combinations of components) and rapidly assay the complex via SDS-PAGE. Furthermore, these constructs can be used as substrates for examining the effects of any point mutation or combination of point mutations we wish. With this powerful tool in hand, we are now able to interrogate MuvB architecture.

Binary interaction between lin9 and p48

In 2006, Harrison et al. observed that a *lin9(n112)* mutant failed to associate with p48 (Harrison, Ceol, Lu, & Horvitz, 2006). The *lin9(n112)* allele is a G241E mutant in a predicted tudor domain (Beitel, Lambie, & Horvitz, 2000), suggesting that this domain physically interacts with p48. To test this, we purified recombinant p48 and lin9^{tudor}, and assayed for interaction by passage over an analytical Superdex S200 column. As shown in Figure 19, we examined peak fractions for the presence of a complex via SDS-PAGE, and none was observed.

Given this result, we repeated the assay in a cellular context, co-infecting Hi5 cells with 6xHis-tagged p48 and GST-lin9 fusions with various truncations (Table 2, Figure 20). Again in these assays, the GST-lin9^{tudor} construct failed to interact with p48, suggesting that post-translational modification or folding issues with bacterially produced lin9^{tudor} is not an issue. Interestingly, a C-terminal deletion of lin9 (lin9$^{\Delta C}$) also interacted with p48, while an N-terminal deletion (lin9$^{\Delta N}$) did not. This suggested that the critical determinants for lin9-p48 association reside within the conserved N-terminus of lin9. However, in vitro GST pulldown assays with a GST-lin9^{N} construct and separately purified p48 failed to show an interaction, regardless of salt concentration, incubation time/temperature, presence or absence of detergent, etc. (data not shown). Finally, we tried using a pre-formed full-length ternary lin9/lin37/ lin52 complex purified from insect cells as bait in an *in vitro* pulldown in the hopes that the presence of additional MuvB components would stabilize the global fold of lin9 and present the p48 binding epitope. Unfortunately, even this ternary complex

was incapable of interacting with p48 *in vitro* (Figure 21a), despite the fact that all four components interact *in vivo* as demonstrated by co-infection and pulldown from lysates (Figure 21b). Interestingly, GST pulldowns from cell lysates expressing GST-lin9^N and 6xHis-p48 did show an interaction, although it is weak (Figure 20). In order to verify that this interaction was real, we subjected the GS4B elution fractions containing 6xHis-p48 and excess GST-lin9^N to nickel affinity chromatography, resulting in the capture of a stoichiometric p48-lin9^N complex as judged by SDS-PAGE (Figure 20). While the efficiency of complex formation *in vivo* between lin9^N and p48 is not high, the complexes that do form appear to be stable during multiple rounds of purification. Taken together, these data suggest that lin9^N is both necessary and sufficient for p48 association in the context of MuvB, as well as suggesting a requirement for co-translational assembly for p48-lin9 complex formation. Because of this, most subsequent biochemical experiments with other MuvB components (unless noted) were performed in insect cells.

Given the stable association between lin9^N and p48, we attempted to further characterize the interaction at the sequence level. The crystal structure of p48 has been solved several times with bound ligands that localize to one of two binding surfaces on the protein. Histone H3 tails have been shown to associate with the top face of p48, and methylation of H3K4 perturbs this binding (Schmitges et al., 2011). Additional interactors with p48 include E(Z)h2, Su(Z)12, and Histone H4, which binds as a monomer to a conserved cleft on the side of p48 (Song, Garlick, &

Kingston, 2008). Interestingly, a short stretch of sequence conservation between lin9^N and histone H4 was noticed (Figure 22a), suggesting that this sequence in lin9 might be responsible for p48 recruitment. However, mutation of these residues to alanine followed by pull-down assays did not disrupt lin9 association with p48 in cells (Figure 22b). Thus, it remains to be seen what the critical binding determinants of p48-lin9^N actually are.

lin52 interactions with MuvB components

lin52 (along with p48) can be expressed alone in insect cells as a GST-fusion. Therefore, we decided to test if purified GST-lin52 was capable of interacting with either the p48-lin9$^{\Delta 93}$ or p48-lin9$^{\Delta C}$ complexes generated in Figure 20. As demonstrated in Figure 23, when approximately stoichiometric amounts of GST-lin52 were added to these complexes, followed by purification over nickel sepharose resin, GST-lin52 associated with p48-lin9$^{\Delta 93}$, but not with p48-lin9$^{\Delta C}$, indicating that lin52 has important interactions with the C-terminus of lin9. This was predicted by the presence of putative coiled-coils in the C-terminal domains of lin9 and lin52 as determined by secondary structure predictions. The C-terminal domain of lin37 is also predicted to form a coiled-coil, so we decided to test if lin52 bound a lin9ΔC construct in the context of other DREAM components. As shown in Figure 24, all full-length components associate, and lin52 remains bound to the MuvB(lin9$^{\Delta C}$) complex as well, suggesting that lin52 has additional contacts with MuvB members, with lin37 being a prime candidate. Additional work supports this, as constructs

containing only the C-terminal domains of lin9, lin37, and lin52 associate on a size exclusion column (Seth Rubin, personal communication). We call this complex MuvB^C.

lin37 interactions with MuvB components

GST-lin37 fusions (Table 2) were generated and tested for their ability to pull down p48-lin9 complexes in *in vivo* pulldown assays. As shown in Figure 25, all GST-lin37 constructs except the extreme C-terminal construct (lin37$^{\Delta NP}$) containing the predicted coiled coil were found to interact with p48-lin9$^{\Delta 93}$. This result leads to three interesting conclusions. First, the fact that the lin37$^{\Delta NP}$ construct cannot bind lin9$^{\Delta 93}$ in the absence of lin52 demonstrates that lin52 is required for C-terminal complex formation, likely by bridging lin9 and lin37, although structural data will be required to confirm this. Second, a lin37$^{\Delta N2}$ construct is capable of binding p48-lin9. Given the poor conservation between lin37 homologs in this region, this result is surprising and may be due to non-specific aggregation. However, this remains to be seen, and in any case, the poor conservation of this central lin37 region does not suggest a function. Therefore, this putative interaction was not pursued. Third and importantly, this experiment shows that the extreme N-terminus of lin37 (lin37$^{\Delta PC}$) is capable of interacting with p48-lin9, suggesting the formation of multiple contacts between lin37 and lin9, in this case likely with the amino-terminus of lin9. Isolation of a subcomplex containing p48, lin9$^{\Delta C}$, and lin37$^{\Delta PC}$ bears this out, as this complex is

stable to purification and concentration, and has shown some promise in initial crystallization screens (Eshwar Ramanan, personal communication).

Functional analysis of lin9^{tudor}

While biochemical analysis of the MuvB complex has been fruitful, these proteins remain, for the most part, uncharacterized. Since its cloning in 2000 (Beitel et al., 2000), lin9 has been annotated as containing a central tudor domain, which represents the best candidate for functional studies as tudor domains are well characterized structurally and functionally

Tudor domains are small, ~50 amino acid domains that fold into a highly compact, 5-stranded beta barrel. Tudor domains play many functional roles during development, from the regulation of the DNA damage response to mRNA processing. Typically, tudor domains bind methylated lysine or arginine side chains, and tudor domain binding of mono-, di-, or tri-methyl lysine and symmetrically or asymmetrically dimethylated arginine has been characterized (Pek, Anand, & Kai, 2012). These modifications are often found in histone tails, and indeed tudor domains are present in many chromatin modifiers or chromatin-bound proteins. Given the presence of a putative tudor domain in lin9, it is tantalizing to speculate that this domain plays some role in localizing the MuvB core to specific modifications, so we attempted to determine if lin9^{tudor} is a histone-binding protein.

In order to determine substrate preference, we expressed a purified ^{15}N-labeled lin9^{tudor} for use in NMR titrations (Figure 26a). By HSQC, lin9tudor is folded,

based on the well-dispersed nature of amide-proton peaks (Figure 26b). In single point titrations, we added a 20-fold molar excess of ligand (either mono-, di-, or tri-methyl lysine). Surprisingly, no significant shifts were observed for any of the ligands. Some small shifts were apparent in the di- and trimethyl-lysine spectra. However, upon assignment of the HSQC it was determined that these shifts (near histidine residues) were due to slight acidification (pH 6.0 from 6.5 starting) from addition of the trimethyl lysine, as these residues also shift when raised to pH 7.0 (Figure 27). While it would be prudent to redo these titrations with more carefully pH'd ligands and with the inclusion of methyl-arginine, parallel array-based approaches suggest that this is not a pressing issue. Briefly, GST-lin9tudor was applied to a commercially available histone peptide array (MODified Histone Peptide Array, ActiveMotif) and probed with anti-GST HRP, revealing no appreciable binding over background (Figure 28). The same construct was sent to Or Gozani's group at Stanford for analysis on their in-house histone peptide arrays, and no binding was detected (Ze Yang, personal communication). Therefore, we conclude that the lin9tudor domain does not bind methylated lysine or arginine, at least in the assays we used.

Given the failure of lin9tudor to bind canonical tudor ligands, we attempted to determine if the tudor domain is important for interaction with other components of MuvB, DREAM, or MMB. Altogether we tested lin9tudor for interaction with p130, B-Myb, lin37ΔN2, and lin52 via biochemical pull-down assays, none of which suggested an interaction (Figure 29).

Structure of lin9[tudor]

As the tudor domain failed to bind ligands, canonical or not, it remained a formal possibility that lin9tudor is not actually a tudor domain. Given its small size, ease of expression, and high-quality HSQC spectrum, we decided to solve the structure of lin9[tudor] in an attempt to shed light on the situation. The overall fold of lin9[tudor] is presented in Figure 30a, alongside the structure of the PHD19 tudor domain (PDB ID 2E5Q). On a gross structural level, the lin9[tudor] domain displays the canonical 5-stranded beta-barrel fold of tudor domains, suggesting that lin9[tudor] is, in fact, a tudor domain. Upon close inspection, however, some structural distinctions are apparent, which may explain why lin9[tudor] fails to bind methylated arginine or lysine residues. First, the binding pocket of lin9[tudor] is sterically occluded relative to that of PHD19[tudor] (Figure 30b). Second, lin9[tudor] lacks an orthogonal arrangement of aromatic amino acids (an 'aromatic cage') required to coordinate hydrophobic methyl groups (Figure30c). Additionally, lin9[tudor] has only two aromatics in the binding pocket, not four, making it highly unlikely that this domain can bind methylated side chains even if these aromatics were accessible and properly oriented.

Discussion

Taken together, the biochemistry presented in this work and in concert with others in the lab has generated the current model of MuvB presented in Figure 31. Briefly, lin9 and lin37 appear to make several direct contacts in pull-down assays, and both contact lin52, which may explain the dependency of lin37 expression on the

presence of lin9 and lin52 (Litovchick et al., 2011). The C-terminal domains of lin9, lin37, and lin52 associate and form a putative triple-helix coiled coil. This represents a possible stable subdomain for crystallization trials. Unfortunately, this complex does not express well in insect cells. Given the fact that lin9 and lin52 interaction can be reconstituted *in vitro*, it is possible that length-optimized constructs (including lin37) could be expressed to high yield in *E. coli*, purified under denaturing conditions, and refolded to form the coiled-coil structure. However, this remains to be tried. The function of the poly-proline region in the middle of lin37 remains a mystery, and further study is needed to identify if the lin37$^{\Delta N2}$-p48-lin9 interaction detected by pull-down assay is real. p48 forms contacts with lin9^N that are likely extensive and require co-translational folding, given our inability to reconstitute this interaction *in vitro*. lin37$^{\Delta PC}$ stacks onto this structure, and given the dependence of lin54 association on lin37 (Seth Rubin, unpublished), it is tantalizing to hypothesize that this N-terminal subcomplex forms a platform for interaction with lin54, although this remains to be tested.

Our structure of lin9^{tudor} has confirmed that this predicted domain possesses a tudor-like fold, but shows clearly the lack of an accessible or complete aromatic cage capable of binding methylated side chains. This has led to questions regarding the real function of this domain, given the conservation of this fold in other lin9 homologs. It is a formal possibility that this domain had an ancestral function in lower organisms that is not required in higher eukaryotes or is compensated for by another MuvB

component. Given the sequence differences between human and *C. elegans* proteins (both with respect to lin9 and globally), it is difficult to use our high-resolution solution structure to make predictions about *C. elegans* lin9^{tudor} function. Therefore, it will be important to assay if *C. elegans* lin9^{tudor} has methylated lysine/arginine-binding ability, either by NMR titration with free modified amino acids or via array-based approaches. As the human tudor domain expresses extremely well, there will hopefully not be a technical barrier to performing these assays.

It is also a possibility that lin9^{tudor} plays a structural role in MuvB assembly. This is partially supported by our observation that p48-lin9$^{\Delta C}$ binary complexes form with alacrity, while p48-lin9^{N} complex formation is inefficient. If crystals of the p48-lin9$^{\Delta C}$-lin37$^{\Delta NP}$ subcomplex diffract to atomic resolution, this structure should address this hypothesis. It will be interesting to see if the p48 structure alone will be sufficient to produce a molecular replacement solution, as lin9 and lin37 have no structural homologs in the PDB. If not, it may be possible to use our high-resolution solution structure of lin9^{tudor} as an additional input for phasing (Mao, Guan, & Montelione, 2011).

Interestingly, we can draw some structural and functional (albeit weak) parallels between MuvB/DREAM and another repressor complex, PRC2. This is motivated by the presence of a common protein component (p48) in both complexes. In the case of PRC2, p48 serves a 'reader' function, as PRC2 nucleates and promotes the spread of repressive H3K27me3 - when this complex reaches an area containing

active chromatin marks (e.g. H3K4me3 and H3K36me2,3), PRC2 is no longer able to bind Histone H3 tails and the spread of PRC2-mediated methylation is stopped (Schmitges et al., 2011). Additionally, the loss of MuvB components on promoters has been associated with a decrease in H3K9me2 marks and a concomitant increase in activating H3K4me3 marks (Sim, Perry, Tharadra, Lipsick, & Ray, 2012). If p48 does not play a large role in the structure and organization of MuvB, it may be possible to use a future atomic resolution structure to engineer lin9 point mutants that fail to bind p48, and ask whether this causes H3K9me2 marks to spread into regions of actively transcribed euchromatin. Additionally, this would suggest that H3K9me2 is actively nucleated by DREAM, which would be one of the first true mechanistic insights into the role of DREAM in gene regulation.

Finally, it has been shown that PRC2 binds a lncRNA called HOTAIR, and that this interaction is important for the repression of the HOXD locus by PRC2 (Rinn et al., 2007). Recently, it has also been shown that tudor-like domains are capable of binding RNA (Shimojo et al., 2008), raising the possibility that lin9tudor may bind ncRNA in order to scaffold chromatin modifiers, a hypothesis that would explain the lack of chromatin modifiers demonstrated by MuDPIT analysis (Litovchick et al., 2007). However tantalizing, this hypothesis is at best speculative and should be approached carefully.

In summary, we have identified stable MuvB subdomains that are amenable to future structural studies, and we have solved the solution structure of the first novel

component of DREAM, the lin9^{tudor} domain. Furthermore, promising crystals of a p48-lin9$^{\Delta C}$-lin37$^{\Delta NP}$ subcomplex represent a step towards a structural understanding of MuvB. While the mechanism of MuvB action remains a mystery, these initial studies have provided several interesting future directions to be pursued.

Materials and Methods

Protein Expression, Purification and Pulldowns

MuvB Proteins

All constructs were cloned into the pFastBac GST-TEV vector and recombinant baculovirus P2 stocks were produced according to standard protocols (Invitrogen). Log-phase Hi5 or Sf9 cells at a density of 2.0 x 10^6 cells/mL in SF900II media (Gibco) were infected with 1mL of indicated P2(s), the culture volume to flask volume ratio never exceeding 1:5. Seventy-two hours post infection, cells were harvested by centrifugation and lysed in a buffer containing 25mM Tris pH 8.0, 200mM NaCl, 5mM DTT, 1x protease inhibitor cocktail (Sigma P8340), and 0.1mM PMSF. Clarified lysates were passed over the indicated resins for either purification or pulldown analysis.

Tudor domain

The lin9 tudor domain was cloned into the pGEV vector and transformed into BL21(DE3) cells for protein expression. 6L culture in LB was induced with 1mM IPTG final and incubated at 25ºC for 16 hours. For NMR labeled preps cells were switched into M9 media containing ^{15}N ammonium chloride with or without ^{13}C

glucose (Cambridge Isotope Laboratories, Inc.) one hour prior to induction. Cells were harvested by centrifugation and lysed in the above buffer lacking inhibitor cocktail. Clarified lysates were passed over GS4B beads, and bound proteins eluted with lysis buffer containing 10mM reduced glutathione. The eluate was diluted threefold with 25mM Tris pH 8.0 (Buffer A), and passed over Source15Q resin (GE Healthcare). Bound proteins were eluted with Buffer A containing 500mM NaCl, then incubated with 2% by total protein weight GST-TEV protease for 16 hours at 10ºC. The cleavage reaction was passed over GS4B resin to remove tags, uncleaved GST-lin9[tudor], and GST-TEV. The tudor domain was concentrated and further purified by passage over a Superdex 75 10/300 sizing column (GE Healthcare) equilibrated with 25mM HEPES buffer pH 7.0 and 100mM NaCl.

NMR Spectroscopy

Purified protein was concentrated to 2mM for structural studies or 0.2mM for binding studies, and 10% by volume D_2O added as a reference. HSQC, HNCO, CBCACONH, CCONH-TOCSY, HCCONH-TOCSY, HCCH-TOCSY, ^{15}N-edited NOESY, and ^{13}C aliphatic/aromatic NOESY spectra were collected at 25ºC on a Varian INOVA 600-MHz spectrometer equipped with an HCN 5-mm cryoprobe. An HNCACB spectrum was obtained using an Avance II 900-MHz spectrometer (Bruker-Biospin) at the Central California 900-MHz NMR facility (Berkely, CA). Spectra were processed with NMRPipe, and analyzed with NMRViewJ, SPARKY,

CYANA, and XPLOR. For binding studies, the indicated amino acid was added to a final concentration of 4mM, for a 20-fold molar excess of ligand to labeled protein.

References

Adams, P. D., Li, X., Sellers, W. R., Baker, K. B., Leng, X., Harper, J. W., et al. (1999). Retinoblastoma protein contains a C-terminal motif that targets it for phosphorylation by cyclin-cdk complexes. *Molecular and cellular biology*, *19*(2), 1068–1080.

Beitel, G. J., Lambie, E. J., & Horvitz, H. R. (2000). The C. elegans gene lin-9,which acts in an Rb-related pathway, is required for gonadal sheath cell development and encodes a novel protein. *Gene*, *254*(1-2), 253–263.

Bremner, R., Cohen, B. L., Sopta, M., Hamel, P. A., Ingles, C. J., Gallie, B. L., & Phillips, R. A. (1995). Direct transcriptional repression by pRB and its reversal by specific cyclins. *Molecular and cellular biology*, *15*(6), 3256–3265.

Broceño, C., Wilkie, S., & Mittnacht, S. (2002). RB activation defect in tumor cell lines. *Proceedings of the National Academy of Sciences of the United States of America*, *99*(22), 14200–14205. doi:10.1073/pnas.212519499

Burke, J. R., Deshong, A. J., Pelton, J. G., & Rubin, S. M. (2010). Phosphorylation-induced conformational changes in the retinoblastoma protein inhibit E2F transactivation domain binding. *The Journal of biological chemistry*, *285*(21), 16286–16293. doi:10.1074/jbc.M110.108167

Burke, J. R., Hura, G. L., & Rubin, S. M. (2012). Structures of inactive retinoblastoma protein reveal multiple mechanisms for cell cycle control. *Genes & development*, *26*(11), 1156–1166. doi:10.1101/gad.189837.112

Burkhart, D. L., & Sage, J. (2008). Cellular mechanisms of tumour suppression by the retinoblastoma gene. *Nature reviews. Cancer*, *8*(9), 671–682. doi:10.1038/nrc2399

Byrne, M., Miller, N., Springer, M., & O'Shea, E. K. (2004). A distal, high-affinity binding site on the cyclin-CDK substrate Pho4 is important for its phosphorylation and regulation. *Journal of molecular biology*, *335*(1), 57–70.

Ceol, C. J., & Horvitz, H. R. (2001). dpl-1 DP and efl-1 E2F act with lin-35 Rb to antagonize Ras signaling in C. elegans vulval development. *Molecular cell*, *7*(3), 461–473.

Ceulemans, H., & Bollen, M. (2004). Functional Diversity of Protein Phosphatase-1, a Cellular Economizer and Reset Button. *Physiological Reviews*.

Chen, H.-Z., Tsai, S.-Y., & Leone, G. (2009). Emerging roles of E2Fs in cancer: an exit from cell cycle control. *Nature reviews. Cancer*, *9*(11), 785–797. doi: 10.1038/nrc2696

Cobrinik, D. (2005). Pocket proteins and cell cycle control. *Oncogene*, *24*(17), 2796–2809. doi:10.1038/sj.onc.1208619

Cohen, P. T. W. (2002). Protein phosphatase 1 – targeted in many directions. *J. Cell Sci.* **115**, 241–256 (2002)

Cohen, P. T., Collins, J. F., Coulson, A. F., Berndt, N., & da Cruz e Silva, O. B. (1988). Segments of bacteriophage lambda (orf 221) and phi 80 are homologous to genes coding for mammalian protein phosphatases. *Gene*, *69*(1), 131–134.

Dahiya, A., Gavin, M. R., Luo, R. X., & Dean, D. C. (2000). Role of the LXCXE binding site in Rb function. *Molecular and cellular biology*, *20*(18), 6799–6805.

Deshaies, R. J., & Ferrell, J. E. (2001). Multisite phosphorylation and the countdown to S phase. *Cell*.

Dick, F. A., Sailhamer, E., & Dyson, N. J. (2000). Mutagenesis of the pRB pocket reveals that cell cycle arrest functions are separable from binding to viral oncoproteins. *Molecular and cellular biology*, *20*(10), 3715–3727.

Dou, Q. P., An, B., & Will, P. L. (1995). Induction of a retinoblastoma phosphatase activity by anticancer drugs accompanies p53-independent G1 arrest and apoptosis. *Proceedings of the National Academy of Sciences of the United States of America*, *92*(20), 9019–9023.

Dunaief, J. L., Strober, B. E., Guha, S., Khavari, P. A., Alin, K., Luban, J., et al. (1994). The retinoblastoma protein and BRG1 form a complex and cooperate to induce cell cycle arrest. *Cell*, *79*(1), 119–130.

Durfee, T., Becherer, K., Chen, P. L., Yeh, S. H., Yang, Y., Kilburn, A. E., et al. (1993). The retinoblastoma protein associates with the protein phosphatase type 1 catalytic subunit. *Genes & development*, *7*(4), 555–569.

Dyson, N. (1998). The regulation of E2F by pRB-family proteins. *Genes & development*, *12*(15), 2245–2262.

Egloff, M. P., Cohen, P. T., Reinemer, P., & Barford, D. (1995). Crystal structure of the catalytic subunit of human protein phosphatase 1 and its complex with tungstate. *Journal of molecular biology*, *254*(5), 942–959. doi:10.1006/jmbi. 1995.0667

Egloff, M. P., Johnson, D. F., Moorhead, G., Cohen, P. T., Cohen, P., & Barford, D. (1997). Structural basis for the recognition of regulatory subunits by the catalytic subunit of protein phosphatase 1. *The EMBO journal*, *16*(8), 1876–1887. doi:10.1093/emboj/16.8.1876

Esterlechner, J., Reichert, N., Iltzsche, F., Krause, M., Finkernagel, F., & Gaubatz, S. (2013). LIN9, a Subunit of the DREAM Complex, Regulates Mitotic Gene Expression and Proliferation of Embryonic Stem Cells. *PloS one*, *8*(5), e62882. doi:10.1371/journal.pone.0062882

Ferguson, E. L., & Horvitz, H. R. (1989). The multivulva phenotype of certain Caenorhabditis elegans mutants results from defects in two functionally redundant pathways. *Genetics*, *123*(1), 109–121.

Ferrell, J. E. (1996). Tripping the switch fantastic: how a protein kinase cascade can convert graded inputs into switch-like outputs. *Trends in biochemical sciences*, *21*(12), 460–466.

Goldberg, J., Huang, H. B., Kwon, Y. G., Greengard, P., Nairn, A. C., & Kuriyan, J. (1995). Three-dimensional structure of the catalytic subunit of protein serine/ threonine phosphatase-1. *Nature*, *376*(6543), 745–753. doi:10.1038/376745a0

Goldbeter, A., & Koshland, D. E. (1981). An amplified sensitivity arising from covalent modification in biological systems. *Proceedings of the National Academy of Sciences of the United States of America*, *78*(11), 6840–6844.

Hagemeier, C., Cook, A., & Kouzarides, T. (1993). The retinoblastoma protein binds E2F residues required for activation in vivo and TBP binding in vitro. *Nucleic acids research*, *21*(22), 4998–5004.

Hanahan, D., & Weinberg, R. A. (2011). Hallmarks of cancer: the next generation. *Cell*, *144*(5), 646–674. doi:10.1016/j.cell.2011.02.013

Harrison, M. M., Ceol, C. J., Lu, X., & Horvitz, H. R. (2006). Some C. elegans class B synthetic multivulva proteins encode a conserved LIN-35 Rb-containing complex distinct from a NuRD-like complex. *Proceedings of the National Academy of Sciences of the United States of America*, *103*(45), 16782–16787. doi:10.1073/pnas.0608461103

Hauser, S., Ulrich, T., Wurster, S., Schmitt, K., Reichert, N., & Gaubatz, S. (2012). Loss of LIN9, a member of the DREAM complex, cooperates with SV40 large T antigen to induce genomic instability and anchorage-independent growth. *Oncogene*, *31*(14), 1859–1868. doi:10.1038/onc.2011.364

Hendrickx, A., Beullens, M., Ceulemans, H., Abt, Den, T., Van Eynde, A., Nicolaescu, E., et al. (2009). Docking motif-guided mapping of the interactome of protein phosphatase-1. *Chemistry & biology*, *16*(4), 365–371. doi:10.1016/j.chembiol.2009.02.012

Henley, S. A., & Dick, F. A. (2012). The retinoblastoma family of proteins and their regulatory functions in the mammalian cell division cycle. *Cell division*, *7*(1), 10. doi:10.1186/1747-1028-7-10

Hiebert, S. W. (1993). Regions of the retinoblastoma gene product required for its interaction with the E2F transcription factor are necessary for E2 promoter repression and pRb-mediated growth suppression. *Molecular and cellular biology*, *13*(6), 3384–3391.

Hiebert, S. W., Chellappan, S. P., Horowitz, J. M., & Nevins, J. R. (1992). The interaction of RB with E2F coincides with an inhibition of the transcriptional activity of E2F. *Genes & development*, *6*(2), 177–185.

Hinds, P. W., Mittnacht, S., Dulic, V., Arnold, A., Reed, S. I., & Weinberg, R. A. (1992). Regulation of retinoblastoma protein functions by ectopic expression of human cyclins. *Cell*, *70*(6), 993–1006.

Horvitz, H. R., & Sulston, J. E. (1980). Isolation and genetic characterization of cell-lineage mutants of the nematode Caenorhabditis elegans. *Genetics*, *96*(2), 435–454.

Huang, H. J., Yee, J. K., Shew, J. Y., Chen, P. L., Bookstein, R., Friedmann, T., et al. (1988). Suppression of the neoplastic phenotype by replacement of the RB gene in human cancer cells. *Science (New York, N.Y.)*, *242*(4885), 1563–1566.

Hurley, T. D., Yang, J., Zhang, L., Goodwin, K. D., Zou, Q., Cortese, M., et al. (2007). Structural basis for regulation of protein phosphatase 1 by inhibitor-2. *The Journal of biological chemistry*, *282*(39), 28874–28883. doi:10.1074/jbc.M703472200

Isaac, C. E., Francis, S. M., Martens, A. L., Julian, L. M., Seifried, L. A., Erdmann, N., et al. (2006). The Retinoblastoma Protein Regulates Pericentric Heterochromatin. *Molecular and cellular biology*, *26*(9), 3659–3671. doi:10.1128/MCB.26.9.3659-3671.2006

Jiao, W., Datta, J., Lin, H.-M., Dundr, M., & Rane, S. G. (2006). Nucleocytoplasmic shuttling of the retinoblastoma tumor suppressor protein via Cdk phosphorylation-dependent nuclear export. *The Journal of biological chemistry*, *281*(49), 38098–38108. doi:10.1074/jbc.M605271200

Kiss, A., Lontay, B., Bécsi, B., Márkász, L., Oláh, E., Gergely, P., & Erdodi, F. (2008). Myosin phosphatase interacts with and dephosphorylates the retinoblastoma protein in THP-1 leukemic cells: its inhibition is involved in the attenuation of daunorubicin-induced cell death by calyculin-A. *Cellular signalling*, *20*(11), 2059–2070. doi:10.1016/j.cellsig.2008.07.018

Knight, A. S., Notaridou, M., & Watson, R. J. (2009). A Lin-9 complex is recruited by B-Myb to activate transcription of G2/M genes in undifferentiated embryonal carcinoma cells. *Oncogene*, *28*(15), 1737–1747. doi:10.1038/onc.2009.22

Knudsen, E. S., & Wang, J. Y. (1997). Dual mechanisms for the inhibition of E2F binding to RB by cyclin-dependent kinase-mediated RB phosphorylation. *Molecular and cellular biology*, *17*(10), 5771–5783.

Knudson, A. G. (1971). Mutation and cancer: statistical study of retinoblastoma. *Proceedings of the National Academy of Sciences of the United States of America*, *68*(4), 820–823.

Korenjak, M., Taylor-Harding, B., Binné, U. K., Satterlee, J. S., Stevaux, O., Aasland, R., et al. (2004). Native E2F/RBF complexes contain Myb-interacting proteins and repress transcription of developmentally controlled E2F target genes. *Cell*, *119*(2), 181–193. doi:10.1016/j.cell.2004.09.034

Lee, C., Chang, J. H., Lee, H. S., & Cho, Y. (2002a). Structural basis for the recognition of the E2F transactivation domain by the retinoblastoma tumor suppressor. *Genes & development*, *16*(24), 3199–3212. doi:10.1101/gad.1046102

Lee, E. Y., Cam, H., Ziebold, U., Rayman, J. B., Lees, J. A., & Dynlacht, B. D. (2002b). E2F4 loss suppresses tumorigenesis in Rb mutant mice. *Cancer Cell*, *2*(6), 463–472.

Lee, W. H., Bookstein, R., Hong, F., Young, L. J., Shew, J. Y., & Lee, E. Y. (1987). Human retinoblastoma susceptibility gene: cloning, identification, and sequence. *Science (New York, N.Y.)*, *235*(4794), 1394–1399.

Lees, J. A., Buchkovich, K. J., Marshak, D. R., Anderson, C. W., & Harlow, E. (1991). The retinoblastoma protein is phosphorylated on multiple sites by human cdc2. *The EMBO journal*, *10*(13), 4279–4290.

Litovchick, L., Florens, L. A., Swanson, S. K., Washburn, M. P., & DeCaprio, J. A. (2011). DYRK1A protein kinase promotes quiescence and senescence through DREAM complex assembly. *Genes & development*, *25*(8), 801–813. doi:10.1101/gad.2034211

Litovchick, L., Sadasivam, S., Florens, L., Zhu, X., Swanson, S. K., Velmurugan, S., et al. (2007). Evolutionarily conserved multisubunit RBL2/p130 and E2F4 protein complex represses human cell cycle-dependent genes in quiescence. *Molecular cell*, *26*(4), 539–551. doi:10.1016/j.molcel.2007.04.015

Lowe, E. D., Tews, I., Cheng, K. Y., Brown, N. R., Gul, S., Noble, M. E. M., et al. (2002). Specificity Determinants of Recruitment Peptides Bound to Phospho-CDK2/Cyclin A. *Biochemistry*, *41*(52), 15625–15634. doi:10.1021/bi0268910

Malumbres, M., Pevarello, P., Barbacid, M., & Bischoff, J. R. (2008). CDK inhibitors in cancer therapy: what is next? *Trends in pharmacological sciences*, *29*(1), 16–21. doi:10.1016/j.tips.2007.10.012

Mao, B., Guan, R., & Montelione, G. T. (2011). Improved technologies now routinely provide protein NMR structures useful for molecular replacement. *Structure (London, England : 1993)*, *19*(6), 757–766. doi:10.1016/j.str.2011.04.005

Margolis, S. S., Walsh, S., Weiser, D. C., Yoshida, M., Shenolikar, S., & Kornbluth, S. (2003). PP1 control of M phase entry exerted through 14-3-3-regulated Cdc25 dephosphorylation. *The EMBO journal*, *22*(21), 5734–5745. doi:10.1093/emboj/cdg545

Meiselbach, H., Sticht, H., & Enz, R. (2006). Structural Analysis of the Protein Phosphatase 1 Docking Motif: Molecular Description of Binding Specificities Identifies Interacting Proteins. *Chemistry & biology*, *13*(1), 49–59. doi:10.1016/j.chembiol.2005.10.009

Mittnacht, S. (1998). ScienceDirect.com - Current Opinion in Genetics & Development - Control of pRB phosphorylation. *Current opinion in genetics & development*.

Morgan, D. O. (1995). Principles of CDK regulation. *Nature*, *374*(6518), 131–134. doi:10.1038/374131a0

Nash, P., Tang, X., Orlicky, S., Chen, Q., Gertler, F. B., Mendenhall, M. D., et al. (2001). Multisite phosphorylation of a CDK inhibitor sets a threshold for the onset of DNA replication. *Nature*, *414*(6863), 514–521. doi:10.1038/35107009

Nelson, D. A., Krucher, N. A., & Ludlow, J. W. (1997). High molecular weight protein phosphatase type 1 dephosphorylates the retinoblastoma protein. *The Journal of biological chemistry*, *272*(7), 4528–4535.

Pardee, A. B. (1989). G1 events and regulation of cell proliferation. *Science (New York, N.Y.)*, *246*(4930), 603–608.

Patwardhan, P., & Miller, W. T. (2007). Processive phosphorylation: mechanism and biological importance. *Cellular signalling*, *19*(11), 2218–2226. doi:10.1016/j.cellsig.2007.06.006

Pek, J. W., Anand, A., & Kai, T. (2012). Tudor domain proteins in development. *Development*, *139*(13), 2255–2266. doi:10.1242/dev.073304

Rayman, J. B., Takahashi, Y., Indjeian, V. B., Dannenberg, J.-H., Catchpole, S., Watson, R. J., et al. (2002). E2F mediates cell cycle-dependent transcriptional repression in vivo by recruitment of an HDAC1/mSin3B corepressor complex. *Genes & development*, *16*(8), 933–947. doi:10.1101/gad.969202

Rinn, J. L., Kertesz, M., Wang, J. K., Squazzo, S. L., Xu, X., Brugmann, S. A., et al. (2007). Functional demarcation of active and silent chromatin domains in human HOX loci by noncoding RNAs. *Cell*, *129*(7), 1311–1323. doi:10.1016/j.cell.2007.05.022

Rogoff, H. A., & Kowalik, T. F. (2004). Landes Bioscience Journals: Cell Cycle. *Cell Cycle*.

Rubin, S. M., Gall, A.-L., Zheng, N., & Pavletich, N. P. (2005). Structure of the Rb C-terminal domain bound to E2F1-DP1: a mechanism for phosphorylation-induced E2F release. *Cell*, *123*(6), 1093–1106. doi:10.1016/j.cell.2005.09.044

Russo, A. A. (1997). Purification and reconstitution of cyclin-dependent kinase 2 in four states of activity. *Methods in enzymology*, *283*, 3–12.

Sadasivam, S., Duan, S., & DeCaprio, J. A. (2012). The MuvB complex sequentially recruits B-Myb and FoxM1 to promote mitotic gene expression. *Genes & development*, *26*(5), 474–489. doi:10.1101/gad.181933.111

Salazar, C., & Höfer, T. (2006). Competition effects shape the response sensitivity and kinetics of phosphorylation cycles in cell signaling. *Annals of the New York Academy of Sciences*, *1091*, 517–530. doi:10.1196/annals.1378.093

Schmit, F., Cremer, S., & Gaubatz, S. (2009). LIN54 is an essential core subunit of the DREAM/LINC complex that binds to the cdc2 promoter in a sequence-specific manner. *The FEBS journal*, *276*(19), 5703–5716. doi:10.1111/j.1742-4658.2009.07261.x

Schmitges, F. W., Prusty, A. B., Faty, M., Stützer, A., Lingaraju, G. M., Aiwazian, J., et al. (2011). Histone methylation by PRC2 is inhibited by active chromatin marks. *Molecular cell*, *42*(3), 330–341. doi:10.1016/j.molcel.2011.03.025

Schulman, B. A., Lindstrom, D. L., & Harlow, E. (1998). Substrate recruitment to cyclin-dependent kinase 2 by a multipurpose docking site on cyclin A. *Proceedings of the National Academy of Sciences of the United States of America*, *95*(18), 10453–10458.

Sherr, C. J., & McCormick, F. (2002). The RB and p53 pathways in cancer. *Cancer Cell*, *2*(2), 103–112. doi:10.1016/S1535-6108(02)00102-2

Shimojo, H., Sano, N., Moriwaki, Y., Okuda, M., Horikoshi, M., & Nishimura, Y. (2008). Novel structural and functional mode of a knot essential for RNA binding activity of the Esa1 presumed chromodomain. *Journal of molecular biology*, *378*(5), 987–1001. doi:10.1016/j.jmb.2008.03.021

Sim, C. K., Perry, S., Tharadra, S. K., Lipsick, J. S., & Ray, A. (2012). Epigenetic regulation of olfactory receptor gene expression by the Myb-MuvB/dREAM complex. *Genes & development*, *26*(22), 2483–2498. doi:10.1101/gad.201665.112

Song, J. J., Garlick, J. D., & Kingston, R. E. (2008). Structural basis of histone H4 recognition by p55. *Genes & development*, *22*(10), 1313–1318. doi:10.1101/gad.1653308

Stengel, K. R., Thangavel, C., Solomon, D. A., Angus, S. P., Zheng, Y., & Knudsen, E. S. (2009). Retinoblastoma/p107/p130 Pocket Proteins: PROTEIN DYNAMICS AND INTERACTIONS WITH TARGET GENE PROMOTERS. *Journal of Biological Chemistry*, *284*(29), 19265–19271. doi:10.1074/jbc.M808740200

Tabuchi, T. M., Deplancke, B., Osato, N., Zhu, L. J., Barrasa, M. I., Harrison, M. M., et al. (2011). Chromosome-Biased Binding and Gene Regulation by the Caenorhabditis elegans DRM Complex. *PLOS Genetics*, *7*(5), e1002074. doi:10.1371/journal.pgen.1002074

Talluri, S., Isaac, C. E., Ahmad, M., Henley, S. A., Francis, S. M., Martens, A. L., et al. (2010). A G1 checkpoint mediated by the retinoblastoma protein that is dispensable in terminal differentiation but essential for senescence. *Molecular and cellular biology*, *30*(4), 948–960. doi:10.1128/MCB.01168-09

Tamrakar, S., & Ludlow, J. W. (2000). The carboxyl-terminal region of the retinoblastoma protein binds non-competitively to protein phosphatase type 1alpha and inhibits catalytic activity. *The Journal of biological chemistry*, *275*(36), 27784–27789. doi:10.1074/jbc.M004542200

Tamrakar, S., Mittnacht, S., & Ludlow, J. W. (1999). Binding of select forms of pRB to protein phosphatase type 1 independent of catalytic activity. *Oncogene*, *18*(54), 7803–7809. doi:10.1038/sj.onc.1203211

Tanoue, T., Adachi, M., Moriguchi, T., & Nishida, E. (2000). A conserved docking motif in MAP kinases common to substrates, activators and regulators. *Nature cell biology*, *2*(2), 110–116. doi:10.1038/35000065

Terrak, M., Kerff, F., Langsetmo, K., Tao, T., & Dominguez, R. (2004). Structural basis of protein phosphatase 1 regulation. *Nature*, *429*(6993), 780–784. doi: 10.1038/nature02582

Thomson, M., & Gunawardena, J. (2009). Unlimited multistability in multisite phosphorylation systems. *Nature*, *460*(7252), 274–277. doi:10.1038/ nature08102

Trimarchi, J. M., & Lees, J. A. (2002). Sibling rivalry in the E2F family. *Nature Reviews Molecular Cell Biology*, *3*(1), 11–20. doi:10.1038/nrm714

Vietri, M., Bianchi, M., Ludlow, J. W., Mittnacht, S., & Villa-Moruzzi, E. (2006). Direct interaction between the catalytic subunit of Protein Phosphatase 1 and pRb. *Cancer cell international*, *6*, 3. doi:10.1186/1475-2867-6-3

Wakula, P., Beullens, M., Ceulemans, H., Stalmans, W., & Bollen, M. (2003). Degeneracy and function of the ubiquitous RVXF motif that mediates binding to protein phosphatase-1. *The Journal of biological chemistry*, *278*(21), 18817–18823. doi:10.1074/jbc.M300175200

Wang, J. Y. J. (1996). Differential Regulation of Retinoblastoma Protein Function by Specific Cdk Phosphorylation Sites. *Journal of Biological Chemistry*, *271*(14), 8313–8320. doi:10.1074/jbc.271.14.8313

Weinberg, R. A. (1995). The retinoblastoma protein and cell cycle control. *Cell*, *81*(3), 323–330.

Wu, J. Q., Guo, J. Y., Tang, W., Yang, C.-S., Freel, C. D., Chen, C., et al. (2009). PP1-mediated dephosphorylation of phosphoproteins at mitotic exit is controlled by inhibitor-1 and PP1 phosphorylation. *Nature cell biology*, *11*(5), 644–651. doi:10.1038/ncb1871

Zhang, H. S., Gavin, M., Dahiya, A., Postigo, A. A., Ma, D., Luo, R. X., et al. (2000). Exit from G1 and S phase of the cell cycle is regulated by repressor complexes containing HDAC-Rb-hSWI/SNF and Rb-hSWI/SNF. *Cell*, *101*(1), 79–89. doi:10.1016/S0092-8674(00)80625-X

Zhang, Z., Zhao, S., Zirattu, S. D., Bai, G., & Lee, E. Y. (1994). Expression of recombinant inhibitor-2 in E. coli and its utilization for the affinity chromatography of protein phosphatase-1. *Archives of biochemistry and biophysics*, *308*(1), 37–41.

Zhu, L., van den Heuvel, S., Helin, K., Fattaey, A., Ewen, M., Livingston, D., et al. (1993). Inhibition of cell proliferation by p107, a relative of the retinoblastoma protein. *Genes & development*, *7*(7A), 1111–1125.
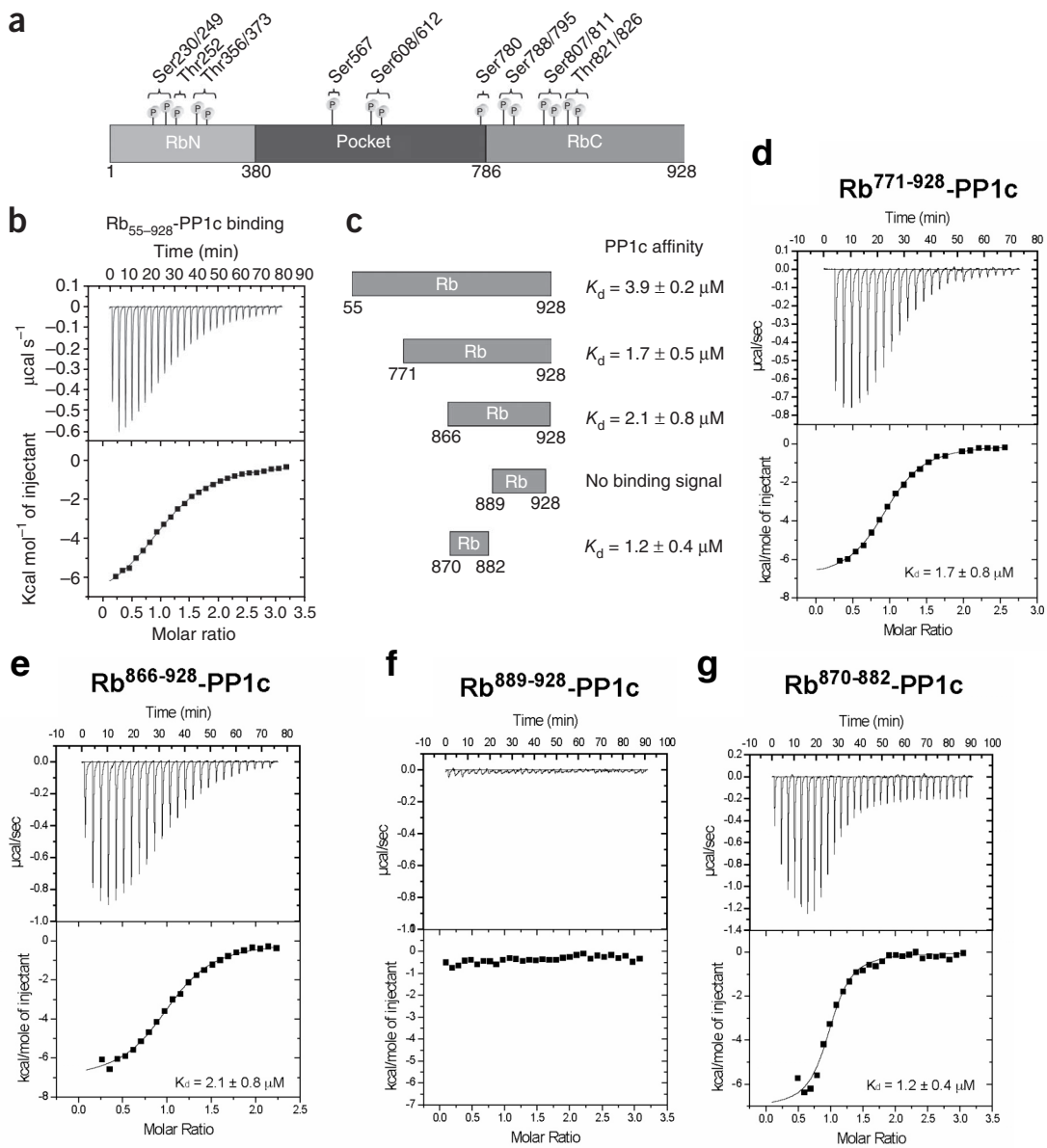
Figure 1 Rb[870–882] is necessary and sufficient for PP1c association. (**a**) Domain structure of Rb with the location of the conserved Cdk consensus phosphorylation sites. (**b**) Isothermal titration calorimetry (ITC) data for titration of Rb[55–928] into PP1c. (**c**) Results from ITC experiments as shown in **b** but with RbC truncation mutants. (**d-g**) ITC data for titration of indicated constructs into PP1c.

Figure 2 Sequence alignment of RbC orthologs from human (hs), mouse (mm), chicken (gg), frog (xl), and fugu (fr). Numbering corresponds to the human sequence. Conservation is shown in yellow and CDK consensus sites are circled. The E2F-DP binding sequence is indicated as well as the amino acids that contact cyclin A (*) and PP1c (+).

Table 1 X-ray data collection and structure model refinement statistics

	Rb$_{870-882}$-PP1c
Data Collection	
Space group	$P4_12_12$
Cell dimensions	
a, b, c (Å)	92.95, 92.95, 192.38
Resolution (Å)	83.6–3.2
R_{pim} (%)[a]	5.6 (20.6)
$I / \sigma I$	18.8 (4.6)
Completeness (%)	98.2 (97.8)
Redundancy	12.3
Refinement	
Resolution (Å)	3.2
No. Reflections	13,588
R_{work} / R_{free} (%)	22.1 / 26.1
No. Atoms	4,798
Protein	4,792
Ligand/ion	6
Avg. B-factor (Å^2)	50.1
R.m.s. deviations	
Bond lengths (Å)	0.004
Bond angles (°)	0.789

Values in parentheses correspond to the highest-resolution shell (3.4–3.2 Å).

[a]$R_{pim} = \Sigma_{hkl} [1/(N-1)]^{1/2} \Sigma_i |I_i(hkl) - I(hkl)| / \Sigma_{hkl} \Sigma_i I_i(hkl)$, where i indexes the ith measurement of reflection hkl and N indicates the total number of times a given reflection is measured.
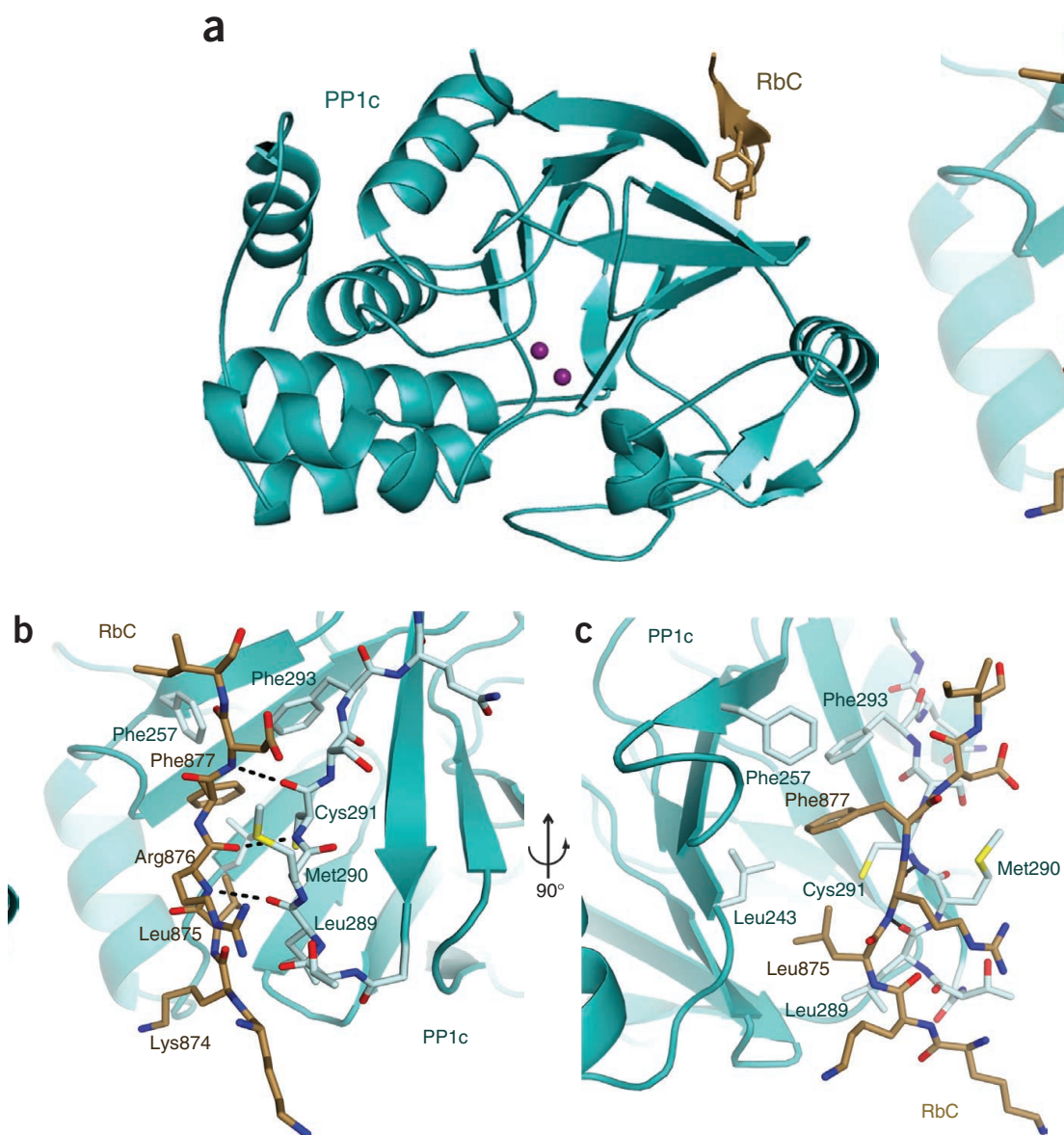
Figure 3 Structure of the Rb[870–882]–PP1c complex. (**a**) RbC (brown) binds in an extended conformation and extends sheet 1 of the PP1c -sandwich domain (cyan). Purple spheres, Mn2+ ions at the distant PP1c catalytic site. (**b**) Close-up view of the Rb[870–882]–PP1c interface. The main chain hydrogen bonding interactions between the RbC peptide (light brown) and PP1c (cyan) are shown. (**c**) Hydrophobic side chain interactions between Rb[870–882] and PP1c.

```
                    |20            |40            |60            |80            |100
PP1c α    1  MSDSEKLNLDSIIGRLLEVQGSRPGKNVQLTENEIRGLCLKSREIFLSQPILLELEAPLKICGDIHGQYYDLLRLFEYGGFPPESNYLFLGDYVDRGKQSLETICLLLAYKIKYPENFFL 120
PP1c β    1  MADG-ELNVDSLITRLLEVRGCRPGKIVQMTEAEVRGLCIKSREIFLSQPILLELEAPLKICGDIHGQYTDLLRLFEYGGFPPEANYLFLGDYVDRGKQSLETICLLLAYKIKYPENFFL 119
PP1c γ    1  MADLDKLNIDSIIQRLLEVRGSKPGKNVQLQENEIRGLCIKSREIFLSQPILLELEAPLKICGDIHGQYYDLLFEYGGFPPESNYLFLGDYVDRGKQSLETICLLLAYKIKYPENFFL 120

                    |140           |160           |180           |200           |220
PP1c α  121  LRGNHECASINRIYGFYDECKRRYNIKLWKTFTDCFNCLPIAAIVDEKIFCCHGGLSPDLQSMEQIRRIMRPTDVPDQGLLCDLLWSDPDKDVQGWGENDRGVSFTFGAEVVAKFLHKHD 240
PP1c β  120  LRGNHECASINRIYGFYDECKRRFNIKLWKTFTDCFNCLPIAAIVDEKIFCCHGGLSPDLQSMEQIRRIMRPTDVPDTGLLCDLLWSDPDKDVQGWGENDRGVSFTFGADVVSKFLNRHD 239
PP1c γ  121  LRGNHECASINRIYGFYDECKRRYNIKLWKTFTDCFNCLPIAAIVDEKIFCCHGGLSPDLQSMEQIRRIMRPTDVPDQGLLCDLLWSDPDKDVLGWGENDRGVSFTFGAEVVAKFLHKHD 240
                                                                          *

                    |260           |280           |300           |320
PP1c α  241  LDLICRAHQVVEDGYEFFAKRQLVTLFSAPNYCGEFDNAGAMMSVDETLMCSFQILKPADKNKGKYGQFSGLNPGGRPITPPR--NSAKAKK- 330
PP1c β  240  LDLICRAHQVVEDGYEFFAKRQLVTLFSAPNYCGEFDNAGGMMSVDETLMCSFQILKPSEKKAKYQYG---GLNSGRPVTPPR--TANPPKKR 327        *  Rb Binding
PP1c γ  241  LDLICRAHQVVEDGYEFFAKRQLVTLFSAPNYCGEFDNAGAMMSVDETLMCSFQILKPAEKKK--------PNATRPVTPPRGMITKQAKK- 323
             *         *                                           * * *
```

Figure 4 Sequence alignment of human PP1c isoforms. The residues involved in Rb binding are conserved in all three paralogs.
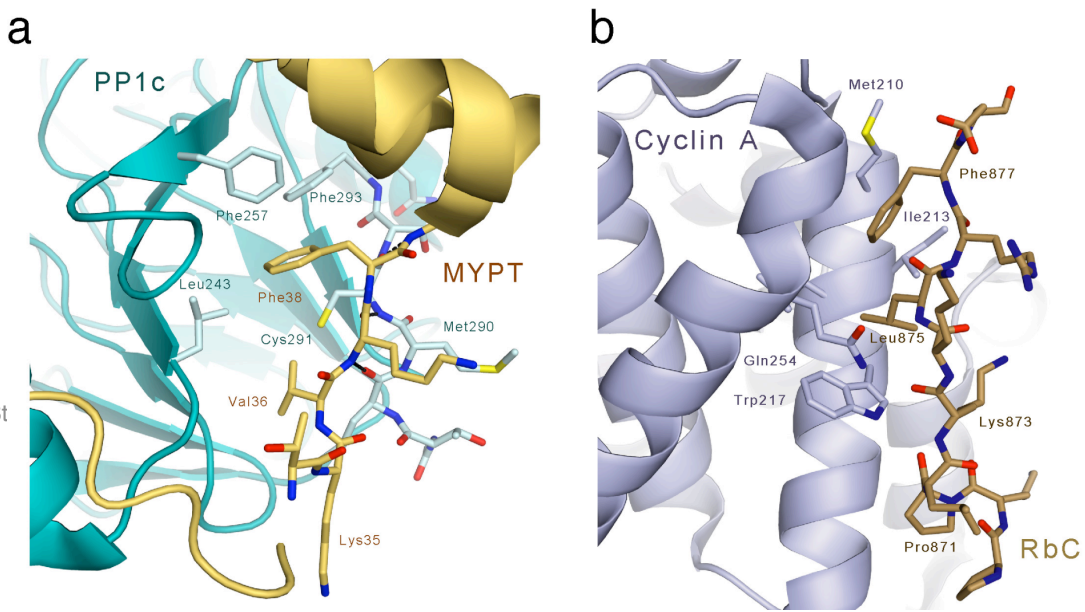
Figure 5 Structural comparison of docking interactions. (**a**) Structure of the myosin phosphatase targeting (MYPT1) subunit (yellow) bound to PP1c. Comparison to the RbC[870-882] structure in Figure 3 shows a similar mode of PP1c binding between Rb and the RVxF motif of PP1c regulatory subunits. (**b**) Structure of an Rb[870-878]-cyclin A-CDK2 complex. Leu875 and Phe877 sidechains in Rb (brown) bind to a hydrophobic cleft in cyclin A (violet).
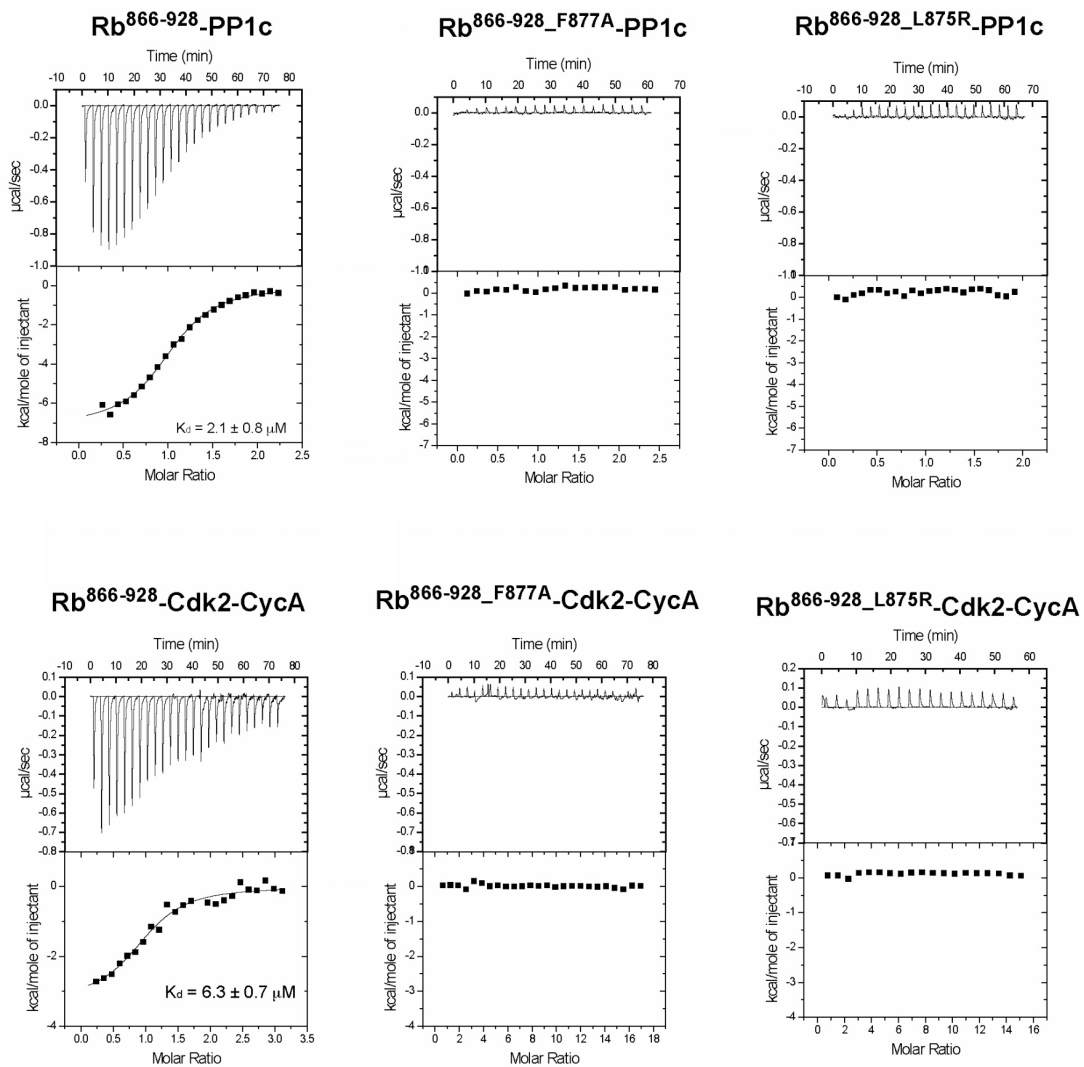
Figure 6 Isothermal titration calorimetry data for titration of Rb[866-928] wild-type and mutants into PP1c or cyclin A-CDK2.
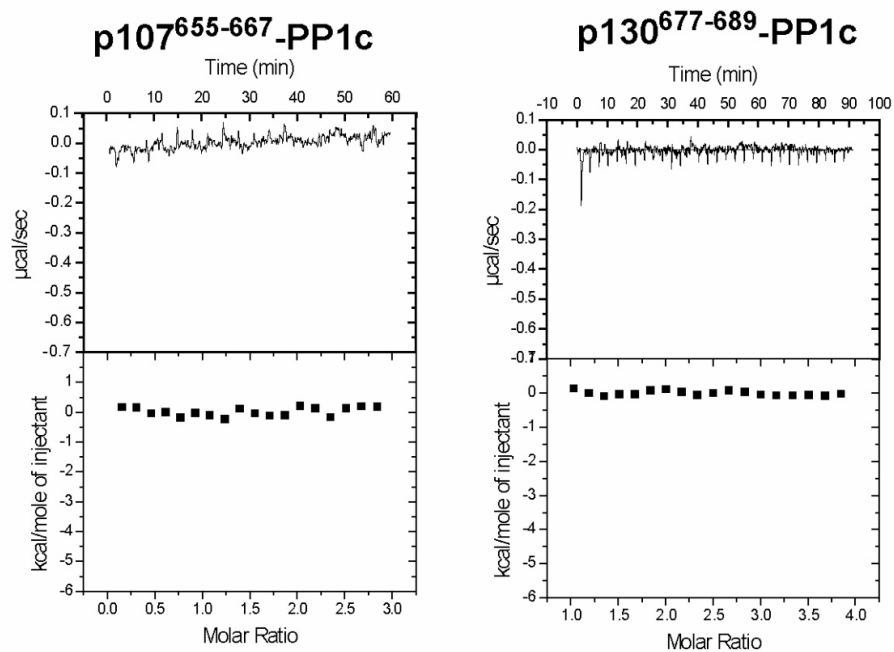
Figure 7 ITC data demonstrating that PP1c does not interact with the p107 and p130 cyclin-CDK recruitment motifs.
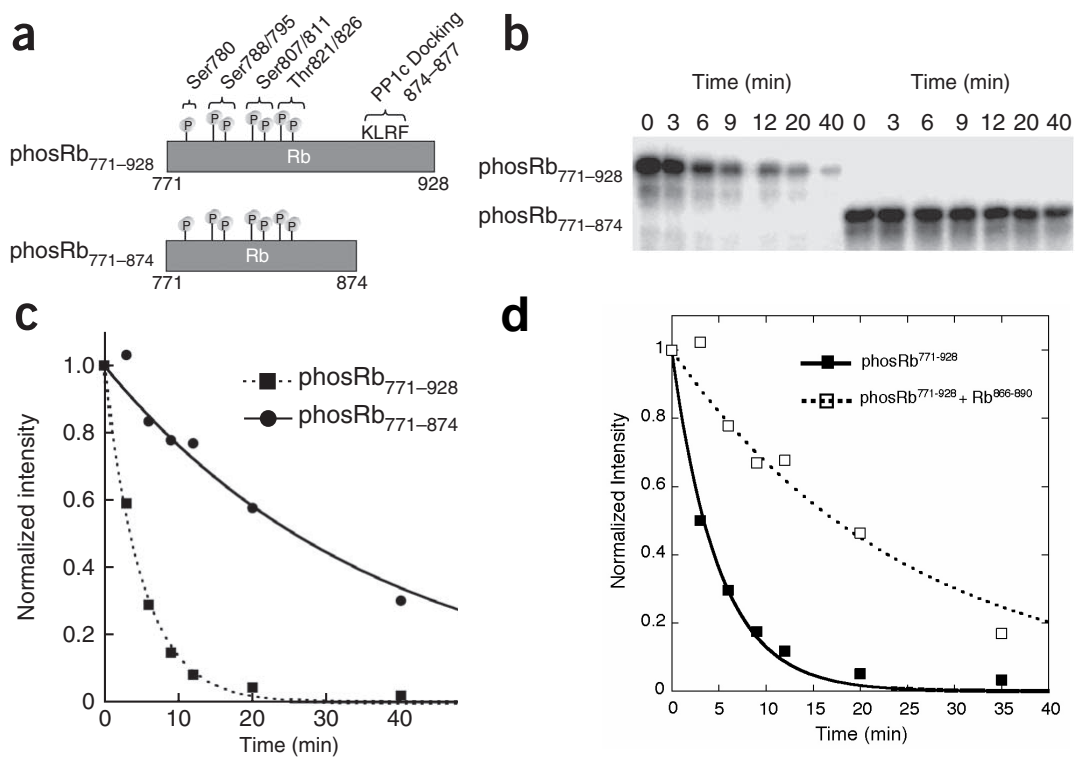
Figure 8 The RbC KLRF docking sequence is required for efficient dephosphorylation by PP1c. (**a**) RbC constructs used as substrates in the phosphatase assays. (**b**) PP1c phosphatase assay using 5µM 32P-labeled phosRb[771-928] and phosRb[771-874] and 10nM PP1c. Quenched aliquots removed from the reaction at the indicated time point are visualized with phosphorimaging. (**c**) Plot of band intensities in **b** as a function of reaction time. (**d**) Plot of RbC dephosphorylation as a function of time with and without saturating quantity of RbC peptide.
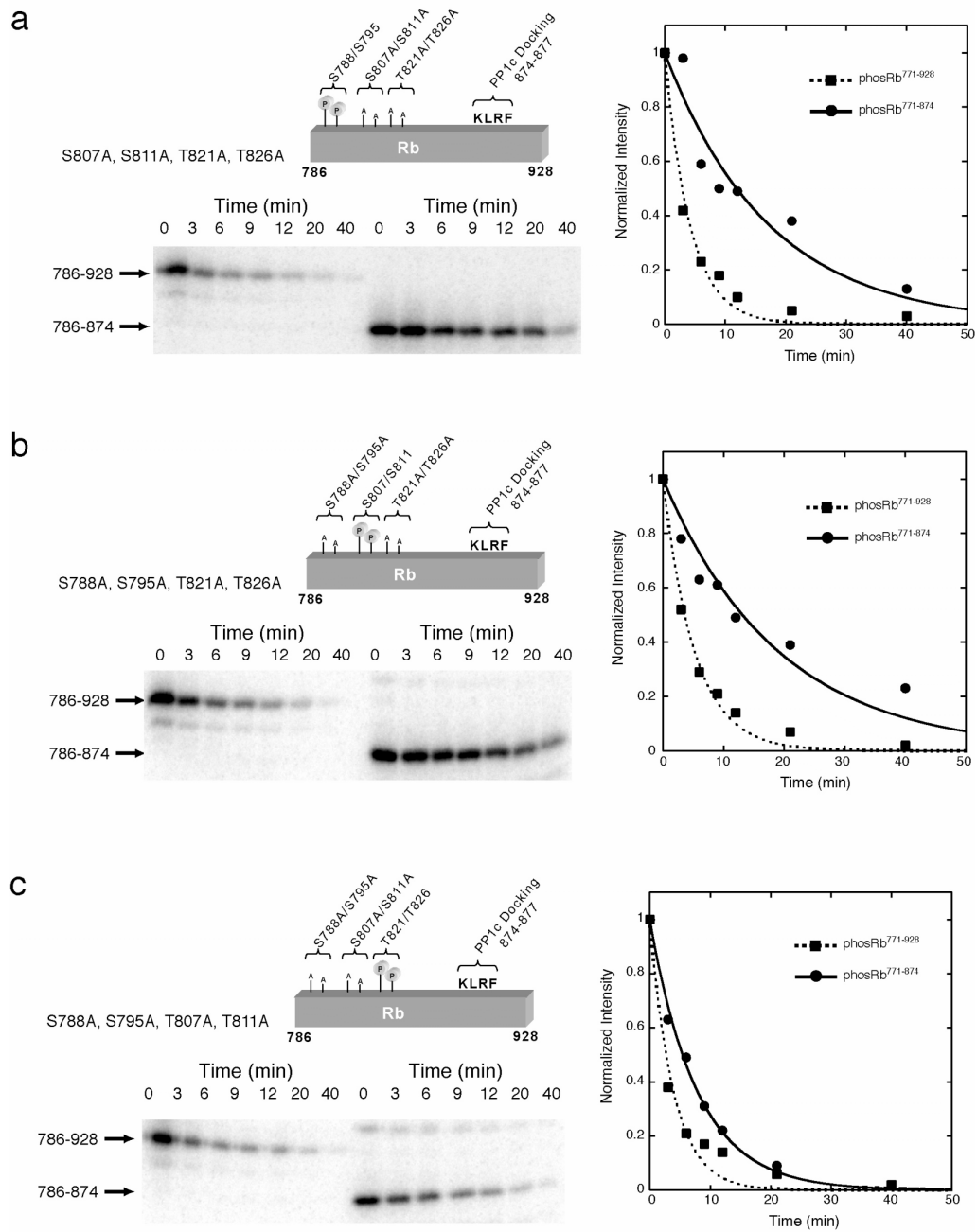
Figure 9 Phosphatase assays on specific phosphoacceptor sites in RbC. (**a**) S788/S795 dephosphorylation. phosRbC$^{786-928}$: $k_{dephos} = 0.24 \pm 0.02$ min^{-1}; phosRbC$^{786-874}$: $k_{dephos} = 0.058 \pm 0.008$ min^{-1}. (**b**) S807/S811 dephosphorylation. phosRbC$^{786-928}$: $k_{dephos} = 0.19 \pm 0.01$ min^{-1}; phosRbC$^{786-874}$: $k_{dephos} = 0.053 \pm 0.006$ min^{-1}. (**c**) T821/T826 dephosphorylation. phosRbC$^{786-928}$: $k_{dephos} = 0.26 \pm 0.03$ min^{-1}; phosRbC$^{786-874}$: $k_{dephos} = 0.128 \pm 0.005$ min^{-1}.
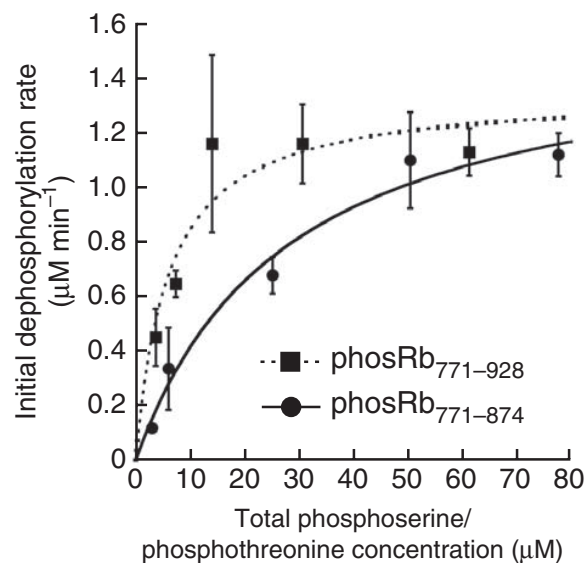
Figure 10 Plot of initial reaction rate as a function of substrate concentration for dephosphorylation of phosRb$^{771\text{-}928}$ and phosRb$^{771\text{-}874}$. Fit of the data to a simple steady-state model indicates similar apparent kcat values, however the apparent Km values are different. Error bars = fitting error for initial rate calculation from time course data.

68
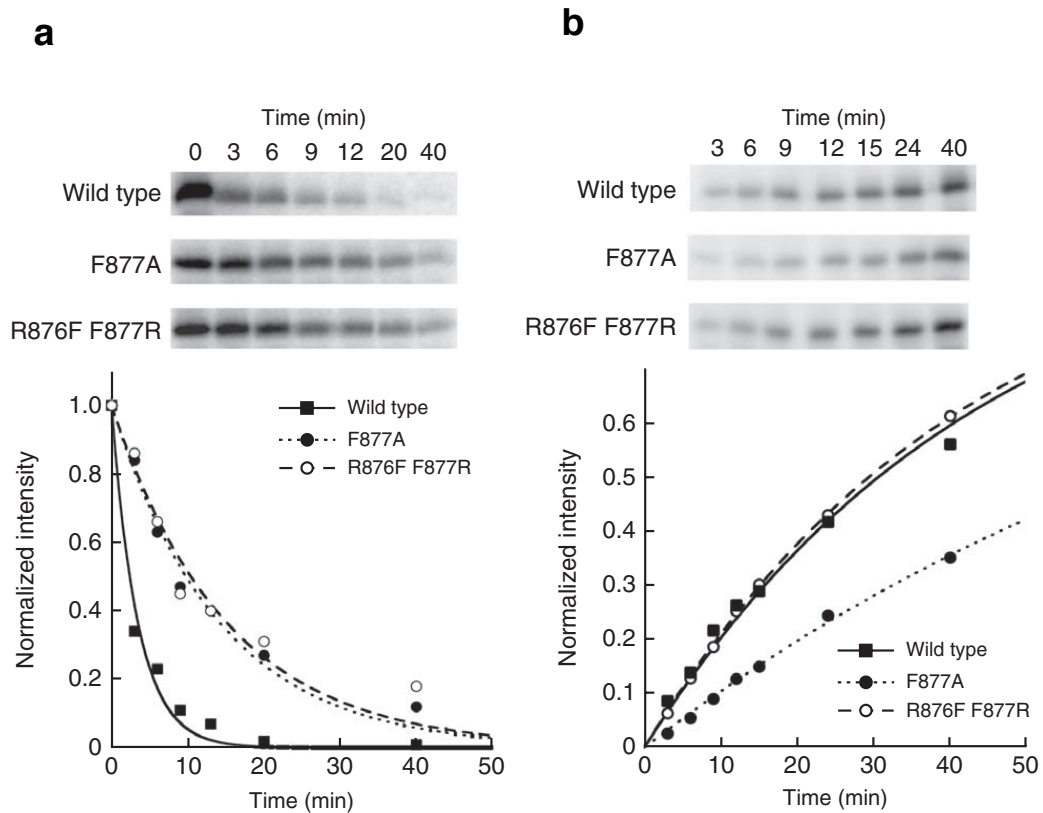
Figure 11 An intact KLRF docking sequence is required for efficient dephosphorylation and phosphorylation. (**a**) Analysis of docking site mutants in the phosphatase assay described in b and c. phosRb[771-928] with the indicated mutation was used as a substrate. (**b**) Analysis of docking site mutants in a kinase assay. Rb[771-928] with the indicated mutation was used as a substrate for cyclin A-CDK2 in the presence of E2F1-DP1.
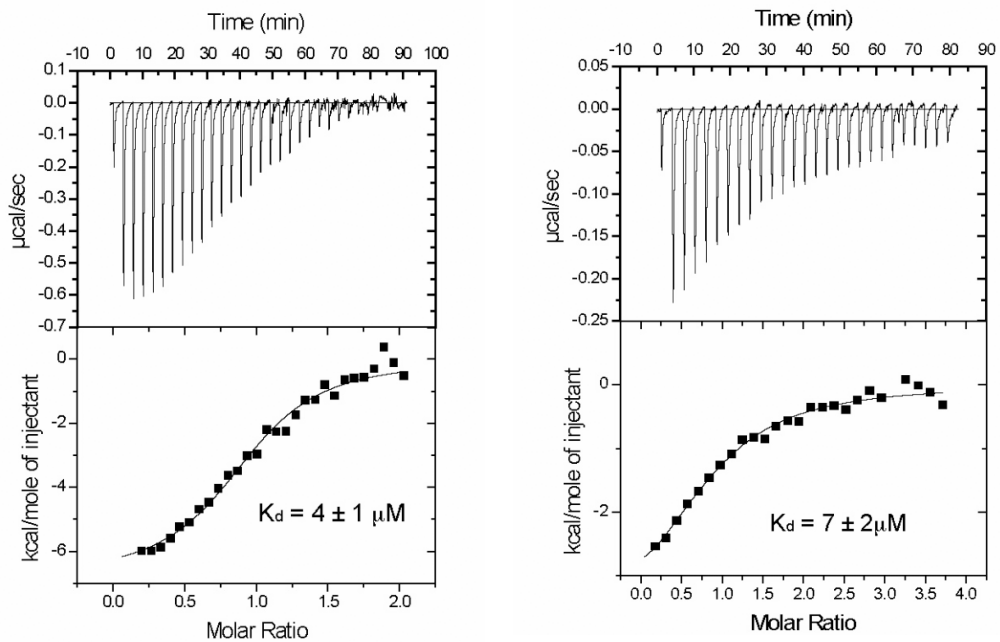
Figure 12 Isothermal titration calorimetry data demonstrating that E2F1-DP1 does not alter the affinity of either PP1c or cyclin A-CDK2 for the Rb docking site
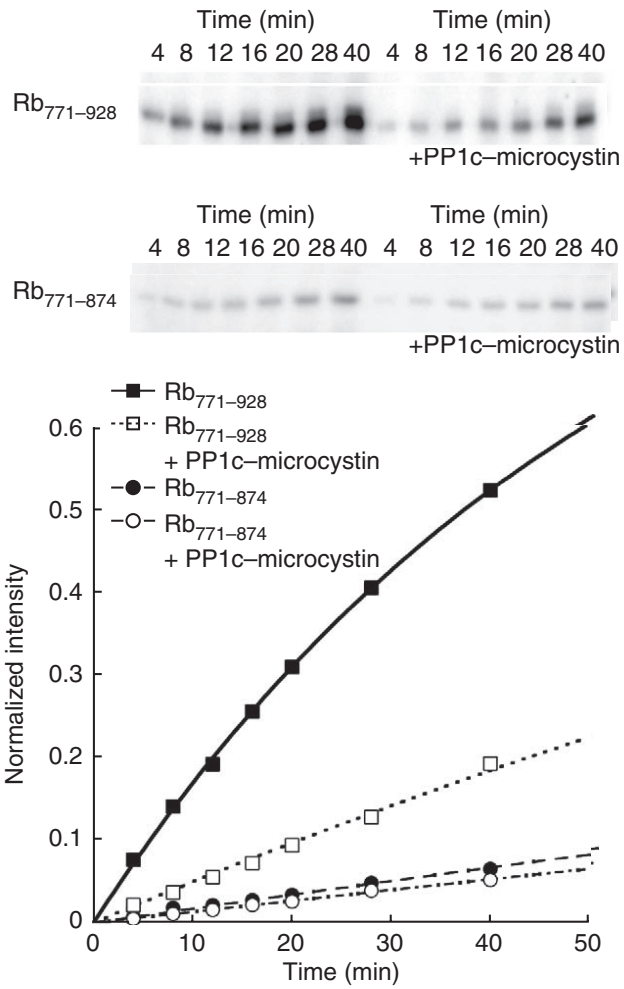
Figure 13 PP1c inhibits cyclin A-CDK2 activity towards RbC. Phosphorylation of 2μM $Rb^{771\text{-}928}$ or $Rb^{771\text{-}874}$ with 75nM cyclin A-CDK2 in the absence and presence of a saturatin concentration of PP1c-microcystin (15μM).
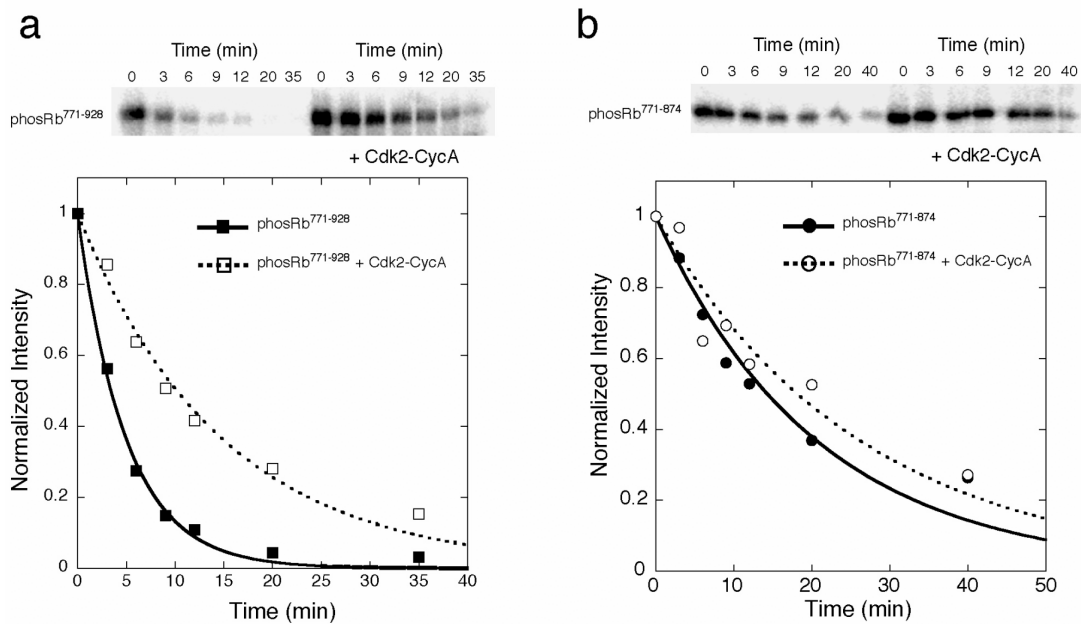
Figure 14 cyclin A-CDK2 inhibits Rb-directed PP1c activity in a docking site dependent manner. In a reaction with PP1c and phosRbC$^{771\text{-}928}$ and without ATP, we characterized the effect of inactive cyclin A-CDK2 on the rate of RbC directed PP1c activity. (**a**) Addition of a saturating quantity of cyclin A-CDK2 inhibits dephosphorylation of phosRbC$^{771\text{-}928}$, reducing the first-order rate constant from $k_{dephos} = 0.20 \pm 0.01$ min^{-1} to $k_{dephos} = 0.068 \pm 0.004$ min^{-1}; this latter rate constant in the presence of kinase is similar to the rate constant for dephosphorylation of phosRbC$^{771\text{-}874}$. (**b**) Addition of cyclin A-CDK2 to the phosRbC$^{771\text{-}874}$ dephosphorylation reaction has little effect on the first order rate constant, changing it from $k_{dephos} = 0.049 \pm 0.004$ min^{-1} to $k_{dephos} = 0.038 \pm 0.005$ min^{-1}.
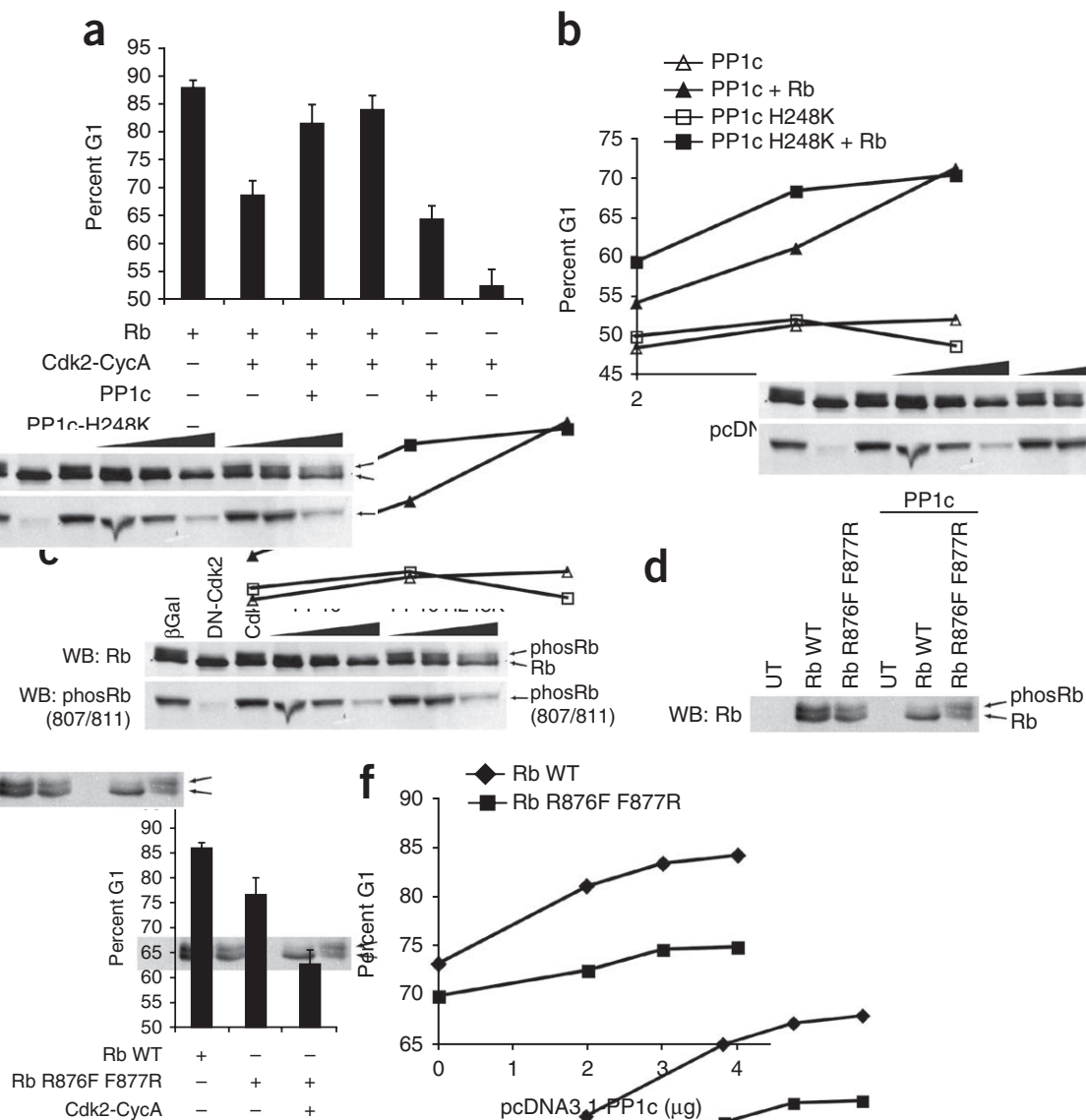
Figure 15 PP1c inhibits CDK inactivation of Rb independently of phosphatase activity. (**a**) Saos-2 cells were transfected with expression plasmids corresponding to the indicated proteins. Error bars, s.d. from the mean from at least four experiments. (**b**) Saos-2 cells were again transfected with cyclin A-CDK2 and Rb expression plasmids and cell-cycle position was analyzed by flow cytometry. The levels of expression plasmid for PP1 and the H248K mutant were titrated to compare their relative effect on an Rb-dependent arrest. (**c**) C33A cells were transfected with the expression plasmids corresponding to the indicated proteins. Rb and phosphoserine 807/811-Rb were detected by western blotting (WB). phosRb and Rb, relative migration positions of hyper- and hypophosphorylated Rb, respectively. (**d**) C33A cells were transfected with the indicated proteins, and Rb was detected as in **c**. WT, wild type. (**e**) Saos-2 cells were transfected with expression plasmids corresponding to the indicated proteins, and the analysis was conducted as in **a**. (**f**) Saos-2 cells were transfected with Rb, or

73

the indicated Rb mutant, and Cdk2-CycA expression plasmids as in **b**. Increasing quantities of PP1c were co-transfected to assess the sensitivity of the Rb mutant to protection from phosphorylation and subsequent cell-cycle advancement out of the G1 phase.
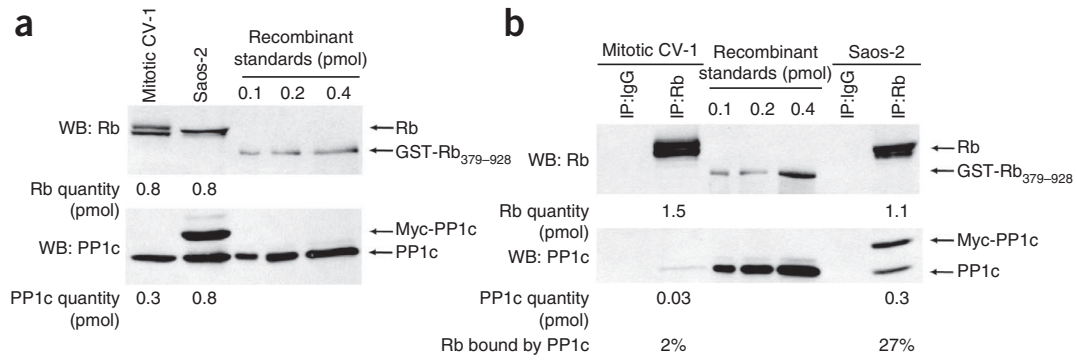
Figure 16 Abundant Rb–PP1c complexes during PP1c-dependent growth arrest. (**a**) Saos-2 cells were transfected as in **Figure 15a** to generate a PP1c-dependent arrest in early G1. CV-1 cells were released form an S-phase block, and mitotic cells were isolated by a mitotic shakeoff 16 h later. Extracts were analyzed by SDS-PAGE and western blotting (WB) to quantitate Rb and PP1c levels. Quantities of Rb and PP1c were determined by band intensities relative to a standard curve generated using recombinant proteins. The quantities are listed below each respective gel lane. (**b**) Rb was immunoprecipitated from extracts prepared as in **a**, and the quantities of Rb and associated PP1c were determined as above.
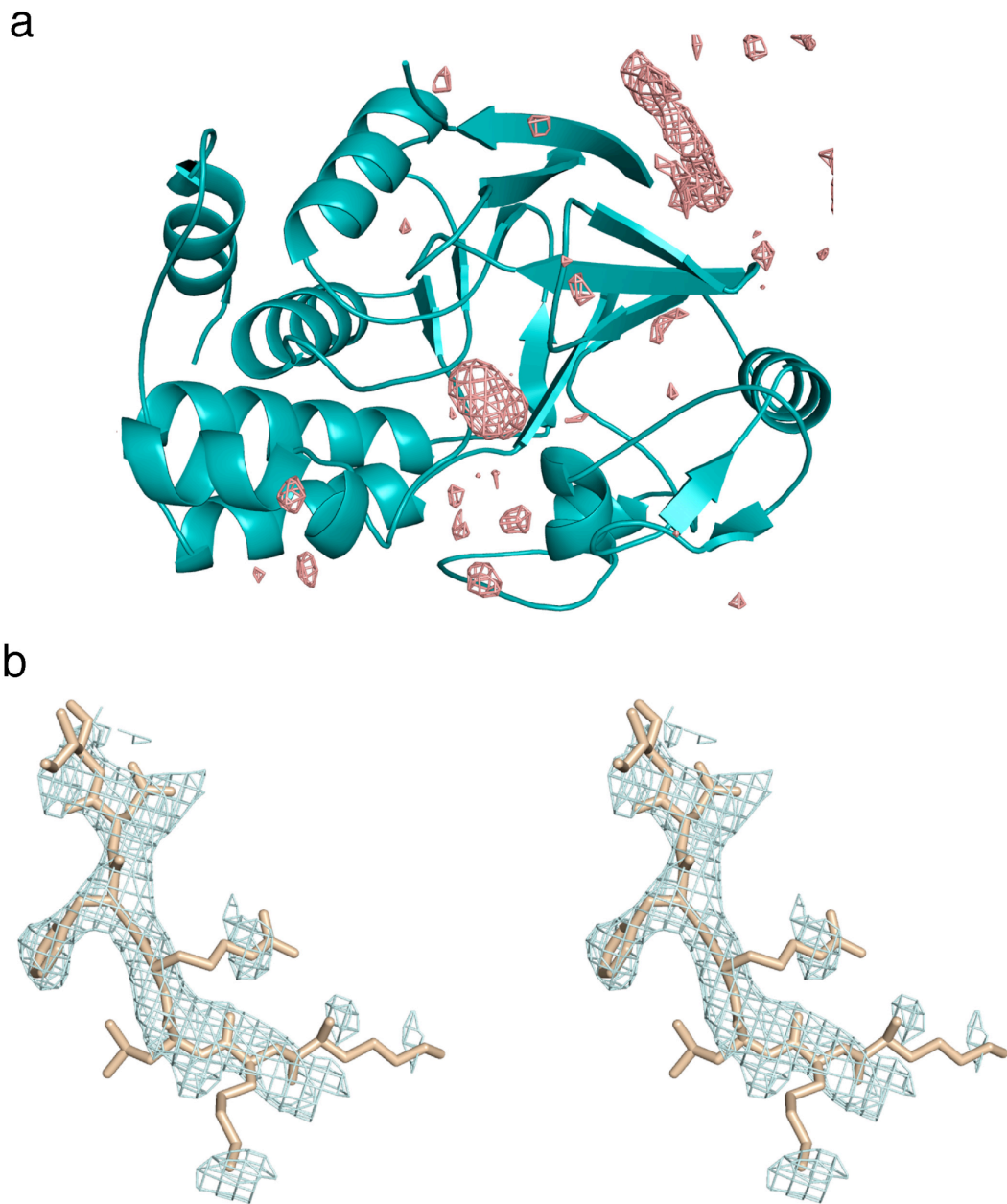
Figure 17 Sample electron density maps. (**a**) Difference map (Fo-Fc; pink) calculated using the experimental structure factors (Fo) and structure factors calculated from the refined PP1c model (Fc) as Fourier coefficients. The map is contoured at 3.5σ. The density peak in the center of the molecule is at the catalytic site and likely corresponds to Mn^{2+} ions left out of the model at this stage of refinement. The significant density at the top right was assigned as the RbC peptide. The PP1c model

is shown in cyan. (**b**) Stereo representation of the RbC peptide (residue 873-879) in the final model. A simulated-annealing omit (Fo-Fc) electron density map (cyan) is contoured at 2σ.
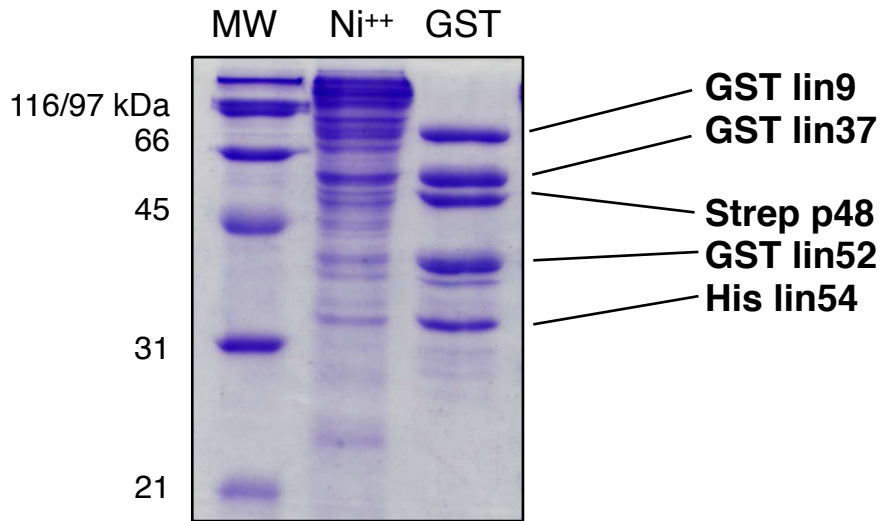
Figure 18 Purification of recombinant MuvB core. Cell extracts of Hi5 cells expressing the indicated constructs were prepared as in methods and MuvB core isolated by nickel sepharose followed by glutathione sepharose affinity chromatography.
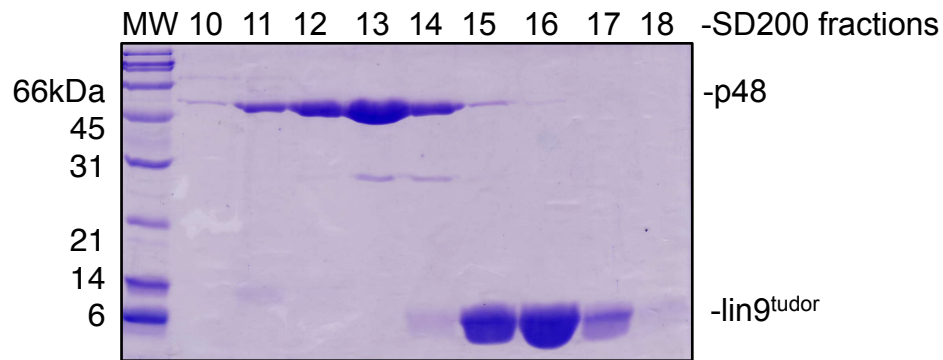
Figure 19 p48 and lin9tudor do not interact in vitro. SDS-PAGE gel of peak fractions from p48 + lin9tudor analytical SD200 column run

Table 2 Summary of GST-lin9 and -lin37 fusion constructs used in this study

construct ID	amino acid boundaries
lin9$^{\Delta 93}$	94-542
lin9$^{\Delta C}$	94-278
lin9$^{\Delta N}$	207-542
lin9^{tudor}	207-278
lin9^{N}	94-207
lin37^{full}	1-248
lin37$^{\Delta C}$	1-198
lin37$^{\Delta PC}$	1-132
lin37$^{\Delta N1}$	93-248
lin37$^{\Delta N2}$	132-248
lin37$^{\Delta NP}$	198-248
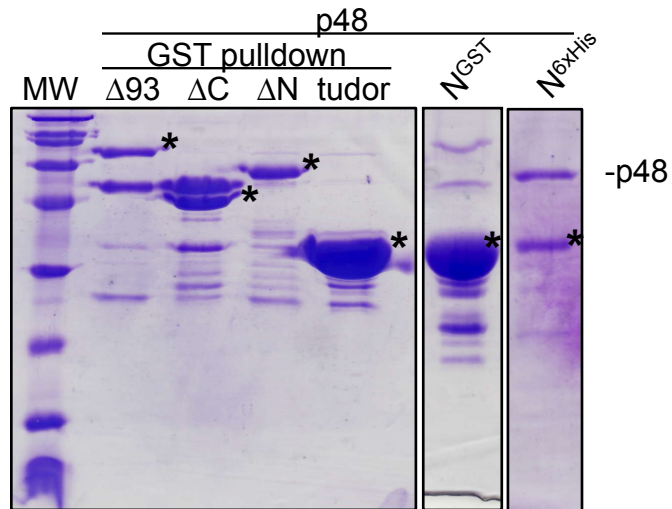
Figure 20 p48 and lin9tudor do not interact i*n vivo*. Hi5 cells were co-infected with indicated GST-lin9 fusions and 6xHis-p48. (*) = position of GST-lin9 fusions.
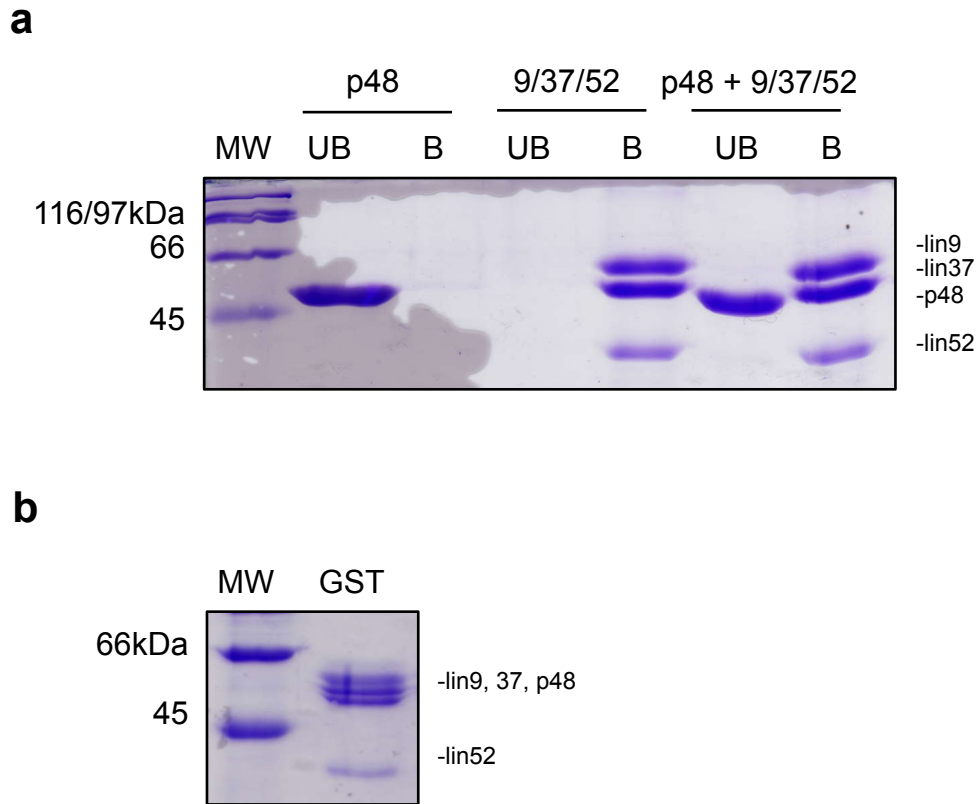
Figure 21 p48 interacts with lin9 in vivo, but not in vitro. (**a**) in vitro p48 pulldowns with pre-formed ternary lin9/lin37/lin52. UB = unbound fraction B = bound fraction. (**b**) GST pulldown of all four components assembled *in vivo*.

a

```
121  WCIYEWFYSNIDKPLFEGDNDFCVCLKESFPNLKTRKLTRVEWGKIRRL--MGKPRRCSS  178  Q5TKA1  LIN9_HUMAN
20   ----------------------RKVLRDNIQGIT--------KPAIRRLARRGGVKRISG   49  P62805  H4_HUMAN
                            *::.:  :.                ****   *  :* *.
```

b
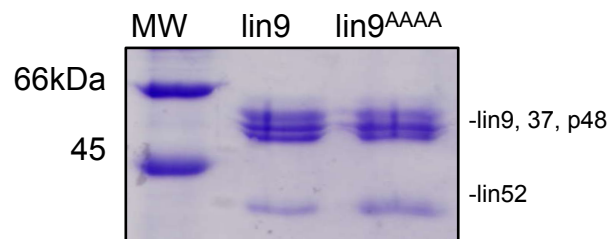
Figure 22 A putative lin9 p48 docking site mutant interacts with p48 *in vivo*. (**a**) Sequence alignment of lin9 with histone H4. Asterisks indicate areas of highest sequence conservation and the characterized H4-p48 docking motif (IRRL). (**b**) Site directed mutagenesis was used to mutate lin9 IRRL to AAAA, followed by *in vivo* pulldowns of wild type and mutant lin9 quarternary complexes.
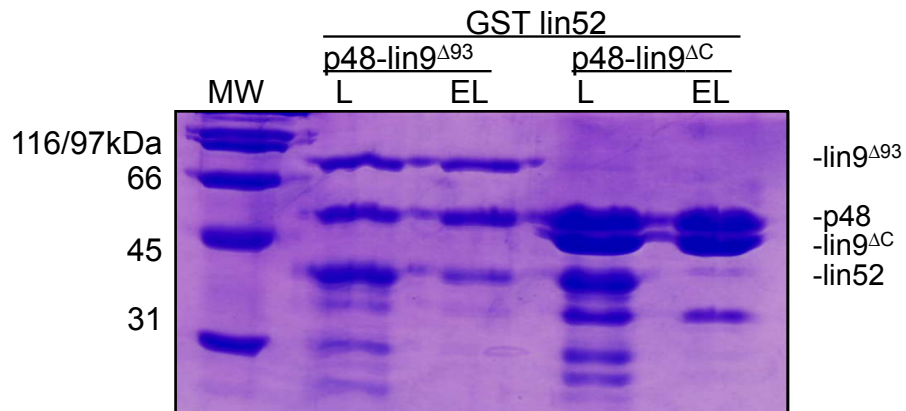
Figure 23 lin52 interacts with the C-terminus of lin9 *in vitro*. L = load, EL = Nickel sepharose resin flow through
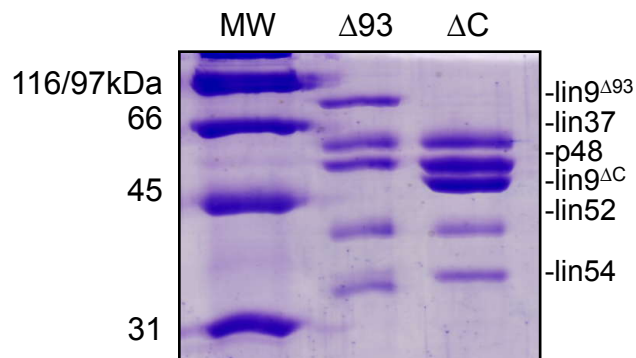
Figure 24 lin52 interacts with the MuvB core in the absence of the C-terminus of lin9. Hi5 cells were infected with indicated lin9 constructs and full length lin37, p48, lin52, and lin52, followed by nickel and glutathione affinity chromatography.
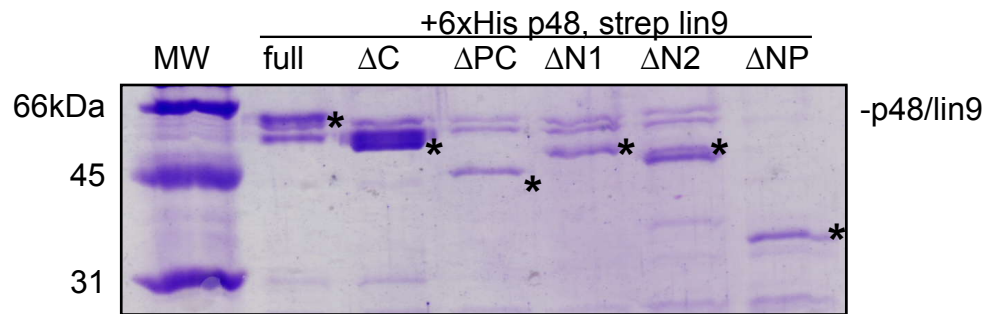
Figure 25 GST-lin37 pulldowns of p48/lin9 from insect cell lysates. Hi5 cells were co-infected with the indicated GST-lin37 fusions and 6xHis p48 and strep tagged lin9, followed by glutathione sepharose pulldown. (*) = positions of GST-lin37 fusions.
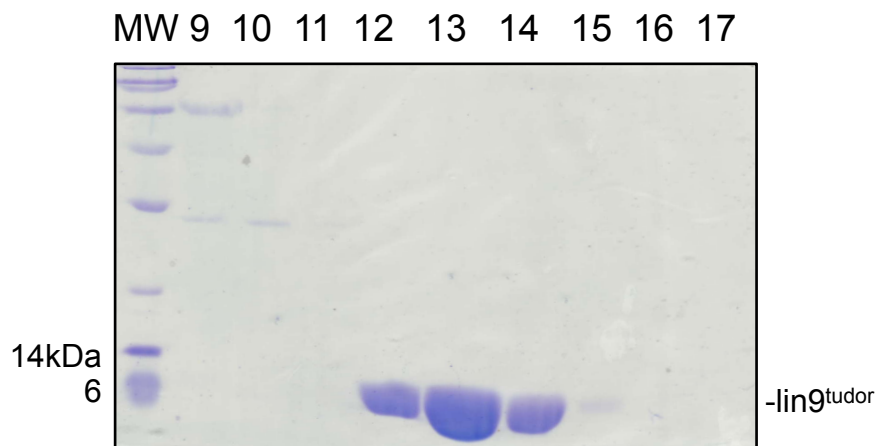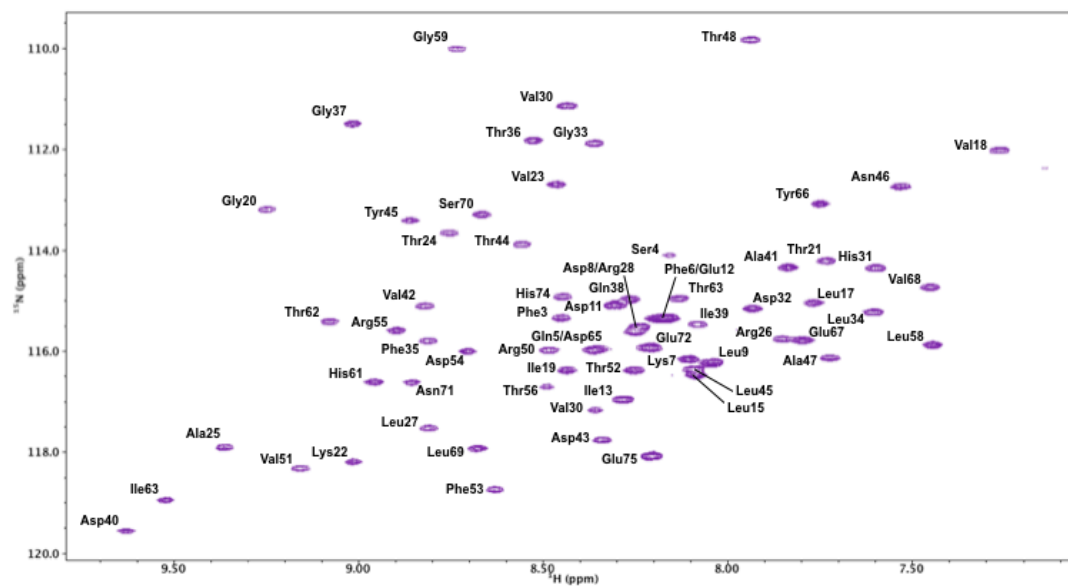
Figure 26 Purification and initial characterization of lin9^tudor. (**a**) SDS-PAGE gel of Superdex 75 fractions containing lin9^tudor. (**b**) 2D-HSQC spectrum of a 2mM lin9^tudor sample in 25mM HEPES buffer pH 7.0 and 100mM NaCl. Amide proton assignments are indicated.
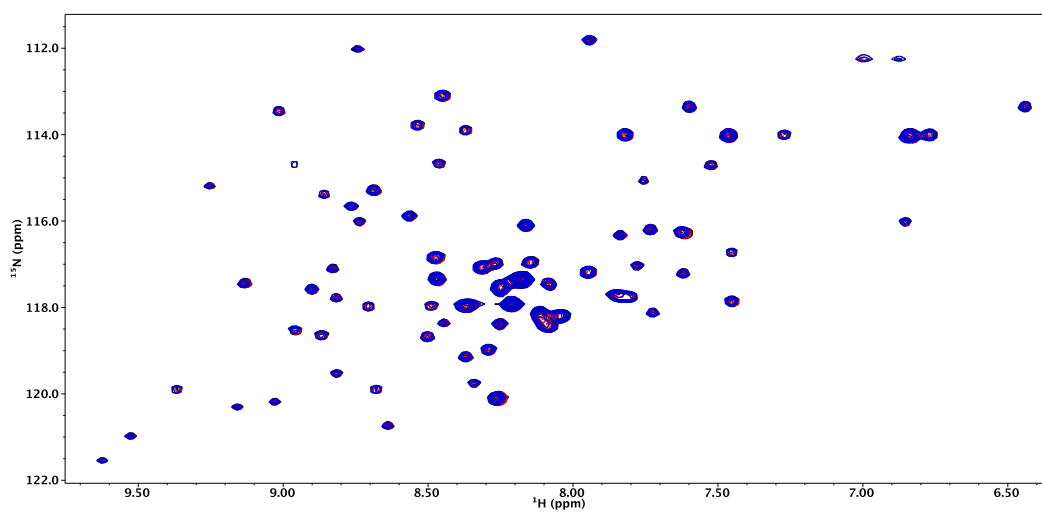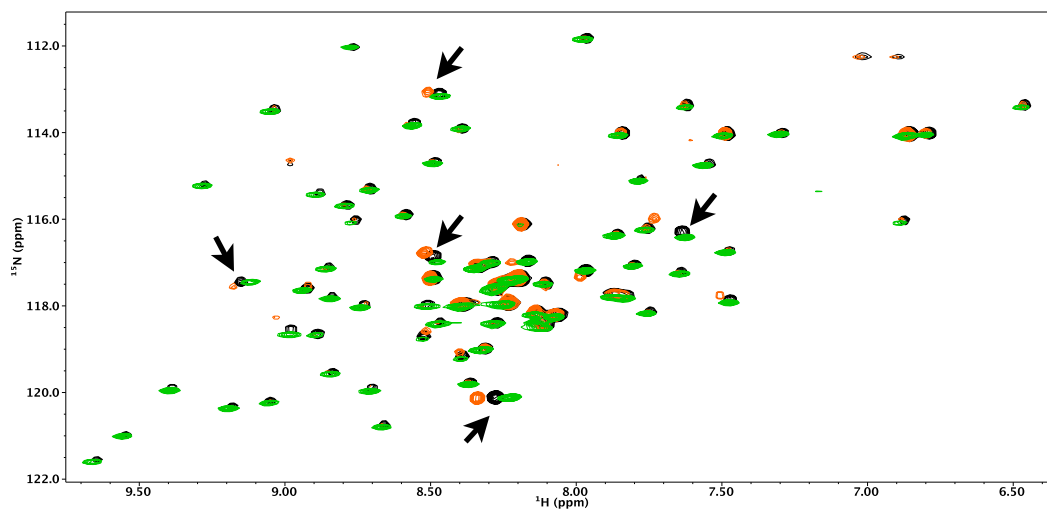
Figure 27 NMR titrations of methylated amino acids into 0.2μM lin9[tudor] (**a**) black = control spectra, red = monomethylated lysine, blue = dimethylated lysine (**b**) black = control, orange = trimethylated lysine, green = pH 7.0 control. pH-dependent shifts discussed in the text are indicated with black arrows.
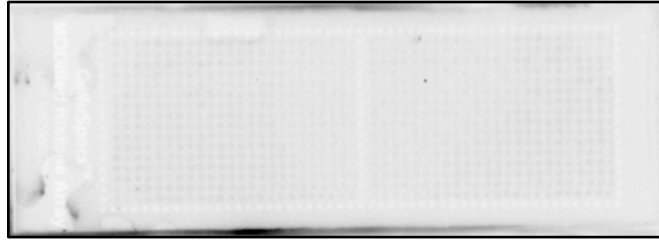
Figure 28 GST-lin9[tudor] does not bind to a MODified Histone Peptide Array (ActiveMotif). The array was probed with 2μM GST-lin9tudor and detected with anti-GST HRP (Santa Cruz) according to product guidelines.
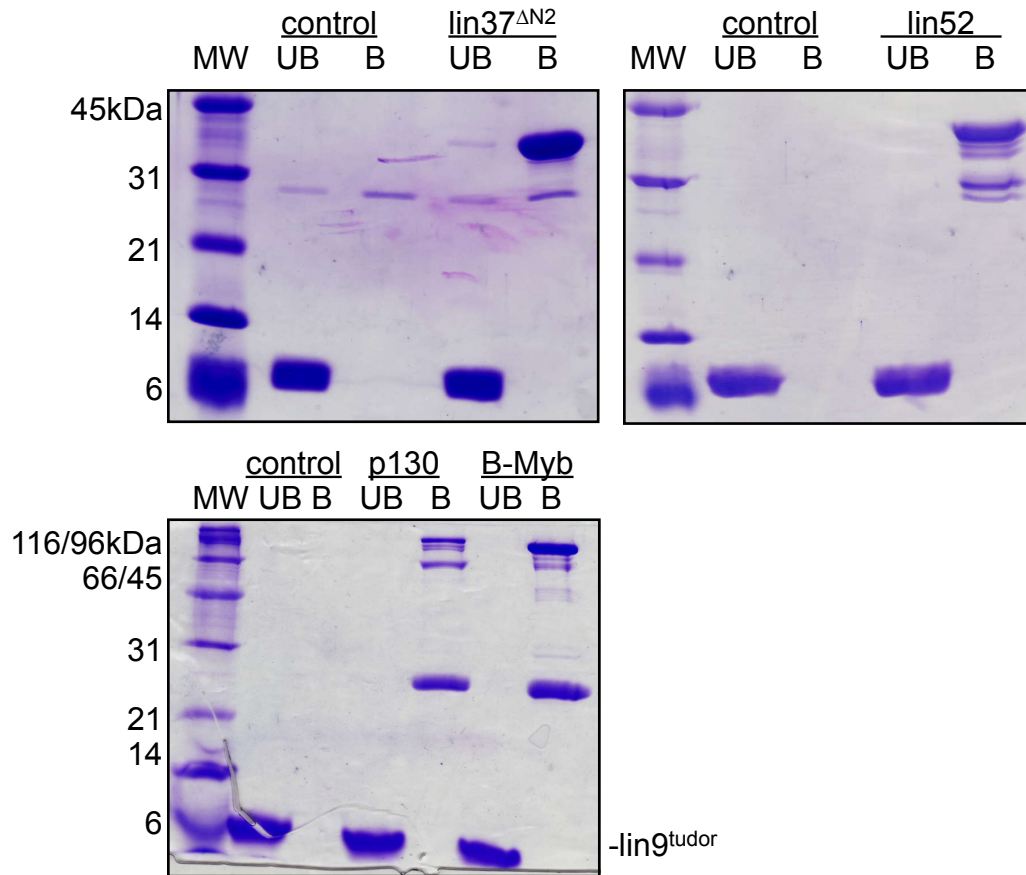
Figure 29 lin9[tudor] *in vitro* pulldowns with indicated GST-fusions. control = beads alone. UB = unbound fraction B = bound fraction.
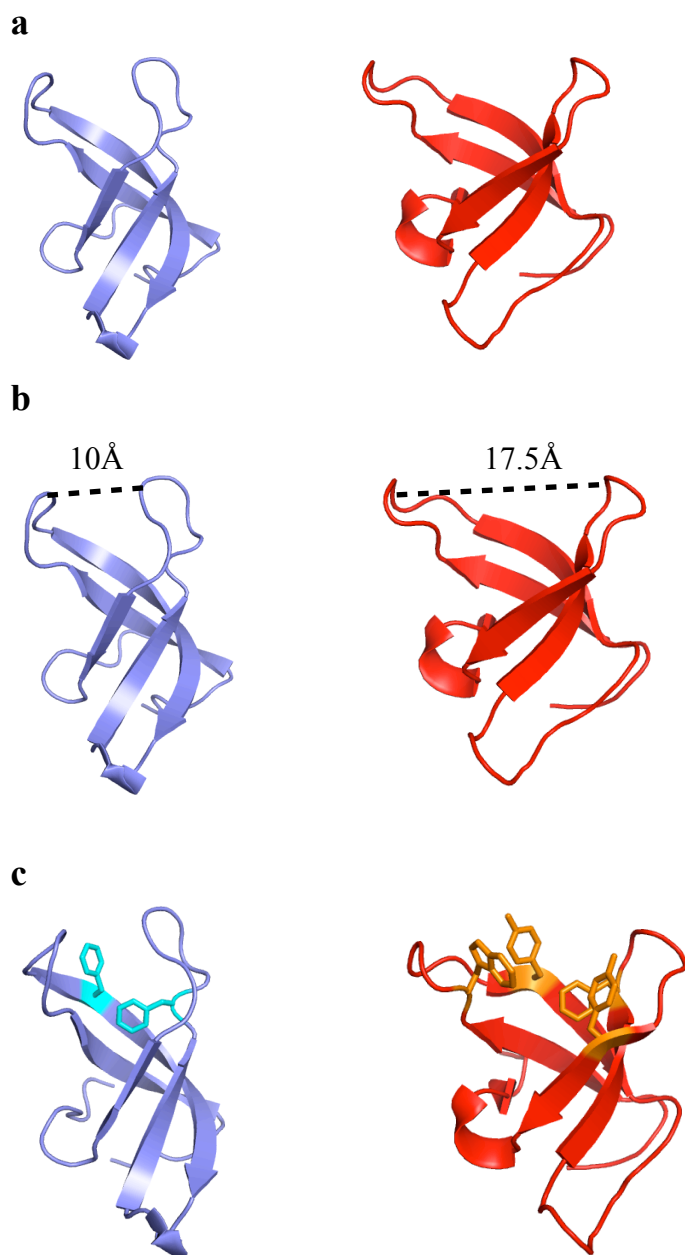
Figure 30 Structure of lin9^tudor and comparison to PHD19^tudor. Blue = lin9^tudor, red = PHD19^tudor. (**a**) comparison of global fold between lin9 and PHD19 tudor domains. (**b**) the putative binding pocket of lin9^tudor is sterically occluded relative to PHD19^tudor. (**c**) comparison of binding pockets, putative lin9 binding pocket residues are shown in cyan, while the known PHD19 binding pocket residues are shown in orange.
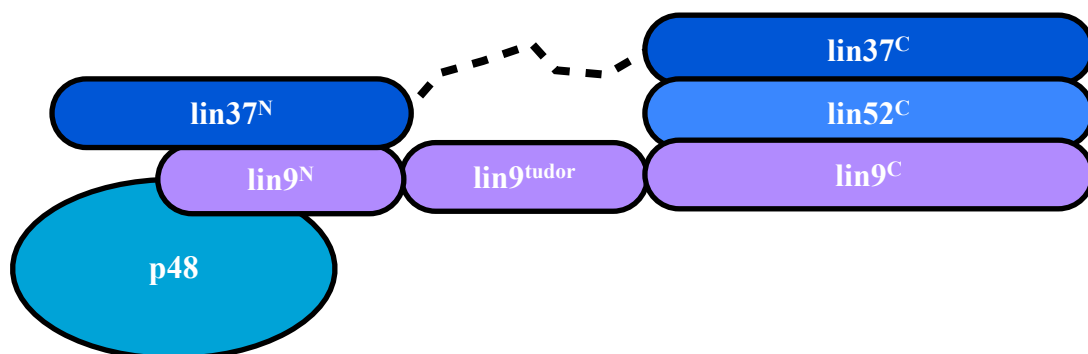
Figure 31 Architecture of the MuvB core. Dashed line = unconserved central lin37 domain. lin54 is left out of this model as its molecular interactions have not yet been determined. It is currently unknown if this complex is further folded, i.e. if the C-terminal coiled coil domain interacts with the N-terminal platform.